Mathematics Thesis
Date of publication: September 28, 2023

A Cellular Potts model of Contact Inhibition of Locomotion.

Author:
Anna Golova
BSc Mathematics
s2483858
Supervisor:
Professor Roeland Merks

Abstract

Contact inhibition of locomotion (CIL) is process whereby cells, upon contact, change their trajectory and move into opposite directions. It plays an important role in a number of biological processes, such as neural crest formation and haemocyte dispersal. In this work, we built an extension to the Act cellular Potts model developed by Niculescu et al. in order to mimic CIL dynamics. Our first aim was to form a minimal model that mimics experimental CIL behaviour. We found that incorporating only repolarisation is sufficient for this, while incorporating only protrusion inhibition is not. Additionally, we found that CIL must be modeled to occur in a probabilistic manner. Secondly, we aimed to see what cell cluster interactions we are able to replicate using our model. While we successfully replicated cell cluster dispersal, we encountered limitations in mimicking haemocyte dispersal in *Drosophila*. Next, we turned to zebrafish stripe formation, where CIL plays a role in the interaction between melanophores and xanthophores, two pigment celltypes. *In vitro*, these cells undergo run-and-chase behaviour with xanthophores pursuing melanophores and melanophores undergoing CIL upon contact. These movements are chiral and always occur at certain angles relative to each other. It is contested whether this interaction occurs *in vivo*, which we aimed to investigate. We first aimed to see what the minimal way was we could model these chiral run-and-chase dynamics and found that changing the direction of melanophore repolarisation was sufficient to replicate the chiral movement in both cells. Secondly, we investigated whether zebrafish stripes could be stable under run-and-chase movements and found that run-and-chase movements disrupt stripe stability. Lastly, we investigated whether chiral movement might contribute to general pattern stability, as suggested by previous research. Our results revealed that simple patterns composed of melanophores and xanthophores were unstable under chiral dynamics, even with inhibited xanthophore movement. Classic cell sorting emerged as a more effective approach for pattern stabilization. In summary, we created a mathematical model of CIL that can be implemented to investigate a range of biological phenomena. By applying this model to study chiral run-and-chase dynamics between melanophores and xanthophores, we deepened the understanding of the role of run-and-chase behaviour in zebrafish patterns and the function of chiral movements in pattern stability.

Contents

Chapter 1

Introduction

Cells display many modes of interaction, which determine their migratory behaviour. One of such modes of interaction is contact inhibition of locomotion (CIL). CIL is a phenomenon whereby two cells, upon collision, change their trajectory and move away from each other [1]. CIL plays an important role in a number of biological processes, including neural crest formation [2], haemocyte dispersal in *Drosophila* [3], and the cerebral cortex development [4]. Thus, understanding CIL can shed light on how these complex processes occur.

Several methods have been used to study CIL, one of which is mathematical modeling. These models have enabled us to simulate complex pattern formation. So far these models have either only focused on the intracellular mechanisms of CIL [5] or looked at its role in pattern formations without studying the intracellular changes that occur [2][6][7]. There is not yet a model that extensively considers both the intracellular mechanisms and their effect on pattern formation.

Here, we aimed to develop a mathematical model of CIL that captures intracellular changes that occur upon cell-contact and that is able to replicate cell cluster dynamics. We did this by extending the Act cellular Potts model developed by Niculescu et al.[8]. Their model captures intracellular changes in actin concentration, which is a protein that is responsible for cell movement and that plays an important role in CIL. By extending upon their work, we were able to investigate which intracellular changes are required for CIL dynamics to occur, whilst also being able to recreate multicellular interactions in which CIL plays a role.

A pattern formation process that we address in this study is stripe formation in the zebrafish *Danio rerio*. Zebrafish stripe formation is made possible by the interaction of two cells; melanophores and xanthophores [9]. *In vitro* these cells show run-and-chase dynamics; xanthophores chase melanophores, while melanophores undergo CIL upon contact with xanthophores and move away from them [9]. These cells always move at certain angles relative to each other and thus show chiral movement.

The role of run-and-chase dynamics *in vivo* has been a controversial topic. Several mathematical models suggest that run-and-chase dynamics could not lead to the zebrafish patterns that we observe [10][11] or that these pattern would not be stable under these dynamics [12]. However, these models have neglected the chiral movement that occurs between melanophores and xanthophores. It has been suggested that chiral movement may facilitate the formation of stable patterns [13], which may be the reason why these models have not succeeded .

In this study we built a cellular Potts model that mimics CIL dynamics. We used this to study the intracellular changes that occur during CIL and to mimic pattern formations in which CIL is involved. With regards to zebrafish stripe formation, we built an *in silico* model of run-and-chase dynamics that show chiral movement. We used this to investigate whether zebrafish patterns could be stable under run-and-chase dynamics and to answer the question of what the role of chirality in cell pattern stability is. Overall, our work extends our understanding of the role of CIL in zebrafish patterns and has formed a model that can be used to study a wide range of patterns in which CIL is involved.

Chapter 2

Biological background

2.1 Mechanisms of contact inhibition of locomotion

Contact inhibition of locomotion (CIL) is the process in which upon contact with another cell, a cell changes its trajectory and moves away [1]. CIL can occur upon contact of a cell with the same celltype (homotypic CIL) or of another celltype (heterotypic CIL). In certain situations involving the collision of cells of different celltypes, only one of the celltypes undergoes CIL. An example of this is melanophore-xanthophore collisions, where only melanophores undergo CIL.

CIL is composed of four steps (Fig. 2.1) [14]. Firstly, the cells recognize that they are in contact with another cell. This is done by forming transient cell-cell adhesions. These cell-cell adhesions then trigger a signalling cascade which inhibits protrusion formation at the front of the cell. Then the cells repolarise and new protrusions form opposite to the cell-cell contact. Finally, the cells separate and move away from each other. Thus, two important parts of CIL are protrusion inhibition, whereby cell movement towards each other is inhibited, and repolarisation, which leads to repulsive cell movement.

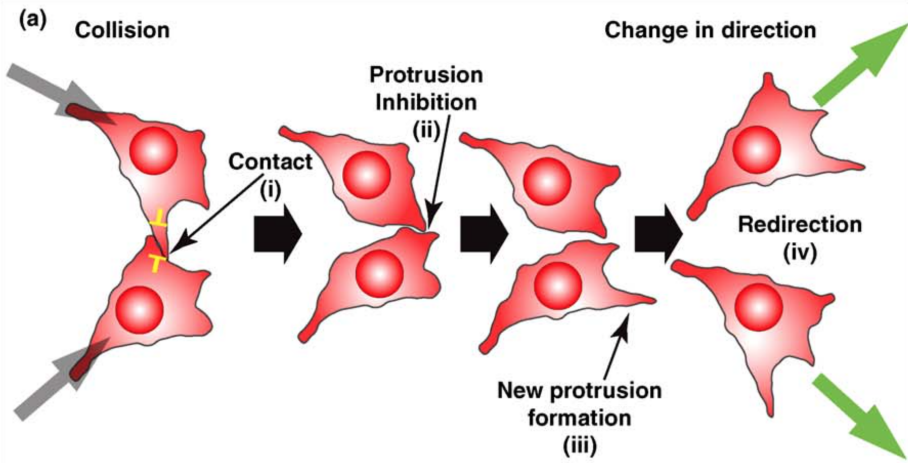

Figure 2.1: **Steps leading to CIL.** First contact between cells occurs (i), which leads to protrusion inhibition (ii). Then new protrusions are made away from the contact site (iii) which lead to redirection of cells (iv). Adapted from [14].

2.2 Zebrafish stripes

Zebrafish have a regular stripe pattern which is formed from three celltypes (Fig. 2.2). Melanophores, containing melanin pigments, are responsible for the formation of dark stripes, while xanthophores, containing yellow pigments, form the light regions [15]. Finally, iridophores, char-

acterized by their reflecting platelets, modulates melanophore and xanthophore survival [15]. Mutants lacking melanophores or xanthophores do not exhibit a normal stripe pattern [4], illustrating their essential role in pattern formation.

Figure 2.2: **Zebrafish have striped patterns.** A picture showing *Danio rerio* and its stripes.

Between these cells, complex interactions occur which influence processes such as cell death, birth, and migration. An example of this is run-and-chase behaviour between melanophores and xanthophores. *In vitro*, its been observed that when xanthophores are placed next to a melanophore, they move towards the melanophore and extend pseudopodia towards them [9]. Upon contact with the xanthophore, the melanophore undergoes CIL, and moves away. This movement is chiral; melanophores circulate xanthophores in a counter-clockwise manner, as illustrated by Fig. 2.3A [9]. Fig. 2.3B shows the specific angles at which this chiral movement occurs by illustrating the relative movement of melanophores and xanthophores. The xanthophores move towards the melanophores at an angle between 0 and 45 degrees, while melanophores run away from xanthophores at an angle between 40 and 160 degrees. The role of this chiral movement is not precisely understood. Structurally, its been shown to occur due to the structure of the actin cytoskeleton [13] and not due to other proteins involved in cell movement, such as microtubules.

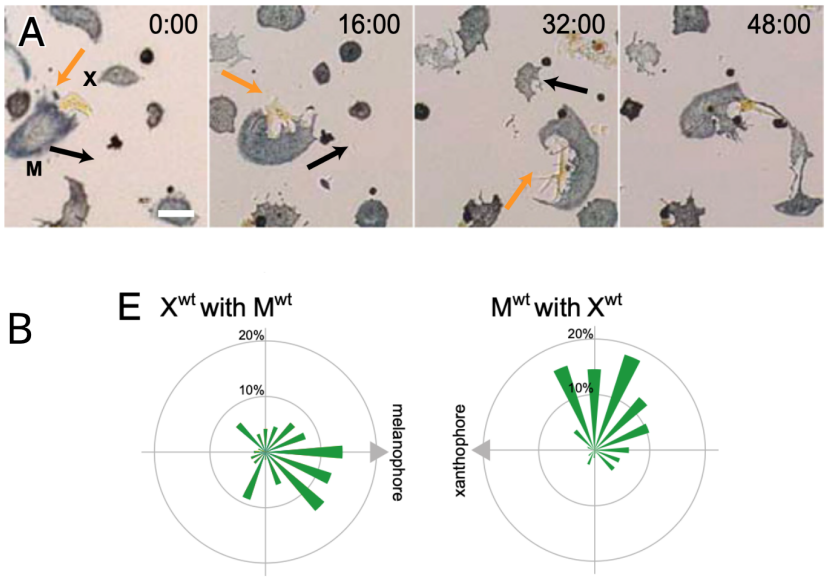

Figure 2.3: **Melanophores circulate xanthophores in a counter-clockwise manner.** A) Movement dynamics between melanophores and xanthophores. The xanthophore reaches for the melanophore by extending pseudopodia. Upon contact, the melanophore undergoes CIL and moves away. The xanthophore then chases the melanophore. B) The relative movement of xanthophores and melanophores. Recordings were made every 4 hours for a 48 hour period. Adapted from [9].

Chapter 3

Methods

3.1 Cellular Potts model

This study was performed using the Cellular Potts model (CPM). The CPM was originally developed by Graner and Glazier to study cell sorting [16]. Essentially, the CPM is a two-dimensional lattice-based model wherein each lattice site is assigned to a particular cell. The dynamics of the lattice composition is governed by the Hamiltonian. The Hamiltonian represents the total energy of the configuration, providing the underlying physical basis for model behaviour.

Every lattice point, represented as u, is designated to a particular cell, expressed by $\sigma(u)$. Each cell is classified into a cell type denoted by $\tau(\sigma(u))$. The medium itself is represented as $\tau(0) = 0$.

At each timestep, the simulation picks a random site u and its neighbouring site v. The cell identity of u is then replicated onto site v and a corresponding change in the Hamiltonian is calculated. This change is either accepted or rejected based on the computed probability:

$$P(\Delta\mathcal{H}) = \begin{cases} e^{-\Delta\mathcal{H}/T} & \Delta\mathcal{H} > 0 \\ 1 & \Delta\mathcal{H} \leq 0 \end{cases} \tag{3.1}$$

Here, T symbolises the system's noise, with a higher T value increasing the change of accepting energetically disadvantageous changes. Time within the model is measured by Monte Carlo Steps (MCS). Every MCS, there are as many copy attempts performed as there are lattice sites on the grid.

The Hamiltonian is expressed as:

$$\Delta\mathcal{H} = \sum_{u,v} J_{\tau(\sigma(u)),\tau(\sigma(v))}(1 - \delta_{u,v}) + \sum_{\sigma} \lambda_A(A_\sigma - A_T(\sigma))^2 + \sum_{\sigma} \lambda_P(P_\sigma - P_T(\sigma))^2$$

In this equation, $J_{\tau(\sigma(u)),\tau(\sigma(v))}$represents the cell adhesion energy, essentially determining the interaction strength between various cell types. $\delta_{u,v}$ is the Kronecker with $\delta_{u,v} = 1$ if $u = v$ and 0 else. $A_T(\sigma)$ signifies the target area of cell σ. If the actual area of the cell (A_σ) differs from the target area, then the effect it wil have on the Hamiltonian is scaled by λ_A. Biologically, λ_A corresponds to the compressibility of the cell. A similar case occurs for the target perimeter $P_T(\sigma)$ of the cell. Here λ_P reflects the stiffness of the cell membrane.

The CPM simulation for this research was implemented using the Tissue Simulation Toolkit. The code used in the simulations is available in Appendix B.

3.1.1 Act extension

An extension to the CPM was developed by Niculescu and de Boer to model cell movement [8]. Each lattice site u has a protrusion activity represented by $Act(u)$, which ranges from 0 to Max_{Act}. Every new lattice site u in the model gets assigned the Act value of $Act(u) = Max_{Act}$.

This value then decreases by 1 for every MCS. Max_{Act} biologically corresponds to the lifetime of the actin polymer.

The contribution of the protrusion system to the Hamiltonian is given by the following:

$$\mathcal{H}_{Act}(u \to v) = \frac{\lambda_{Act}}{Max_{Act}} \left(\left(\prod_{u' \in V(u)} Act(u') \right)^{1/|V(u)|} - \left(\prod_{v' \in V(v)} Act(v') \right)^{1/|V(v)|} \right)$$

This term is subtracted from the Hamiltonian. The term shows that it is copy attempts from an active sites unto an inactive site is favoured. Here $V(u)$ represents the Moore neighbourhood of u which belongs to the same cell as u. In the equation, λ_{Act} represents maximum contribution of the Act model to the Hamiltonian. Biologically, it corresponds to the protrusion strength of the actin polymers.

3.1.2 CIL extension

Two important changes occur to a cell during CIL. Firstly, following cell-cell contact, the protrusions of the cell get inhibited. Thus, the actin concentration near the contact site decreases. Fig. 3.1 visualizes how this is incorporated into the model. Upon cell-cell contact, the Act value of the contact site is set to 0. The Act value of all neighbours within of the degree $I_R - 1$ is also set to 0, whereby I_R is termed the inhibition radius.

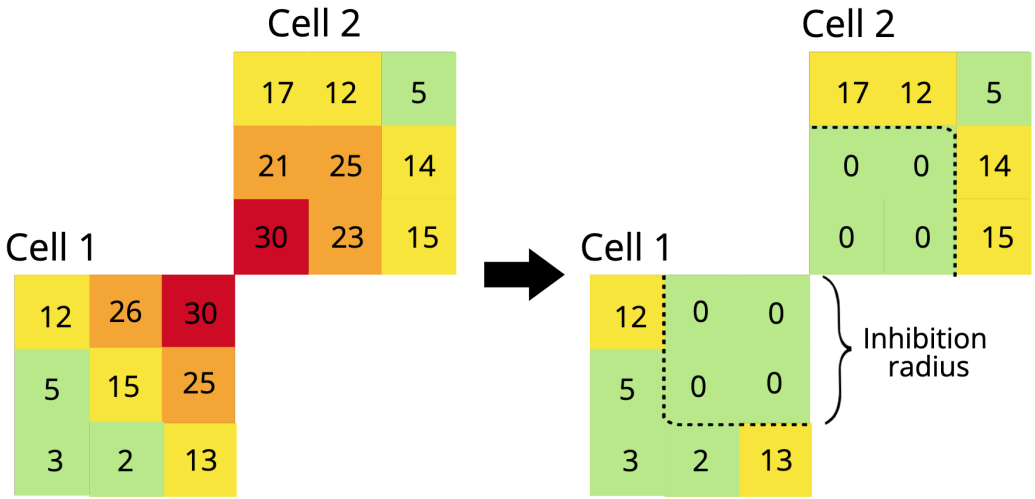

Figure 3.1: **Protrusion inhibition implementation.** Colours and numbers within the squares represent the Act value of the site, ranging from 0 (green) to Max_{Act} (red). Upon contact of two cells, all squares within a certain radius of the contact site (termed the inhibition radius) receive an Act value of 0.

The second major intracellular change that occurs during CIL is the repolarisation of the cell. This implies that the actin concentration of the cell opposite to the cell-cell contact site. Fig. 3.2 shows how repolarisation is incorporated into the model. When site T makes contact with another cell, the vector $\vec{v} = C - T$ is computed, whereby C denotes the centre of the cell (Fig. 3.2A). The unit vector $\vec{u}$ of $\vec{v}$ is used to find the site opposite to C. From C, the code performs steps of $\vec{u}$, until it finds a site located at the edge of the cell (Fig. 3.2B). This is the site opposite to C and is termed R. The Act value of R is set to Max_{Act} (Fig. 3.2C). The following algorithm is then used to fill the sites next to R:

for $i = 1$, i++, while $i <$ the maximum cell length **do**
  for $j = 1$, j++, while $j <$ the maximum cell length **do**
    $X_1 = R - j \cdot \vec{u} + i \cdot \vec{u}^{\perp}$
    $X_2 = R - j \cdot \vec{u} - i \cdot \vec{u}^{\perp}$
    if X_1 belongs to the same cell as R **and** $Act(X_1) < Max_{Act} - (i + j)$ **then**

$Act(X_1) = Max_{Act} - (i + j)$
end if
if X_2 belongs to the same cell as R **and** $Act(X_2) < Max_{Act} - (i + j)$ **then**
$Act(X_2) = Max_{Act} - (i + j)$
end if
end for
end for

Within this algorithm, X_1 and X_2 are two sites near R. The term $-(i+j)$ within the if-statement ensures that the act value of the sites is increased less if they are further away from R. This algorithm ensures that sites are filled in proportion to how close they are to R.

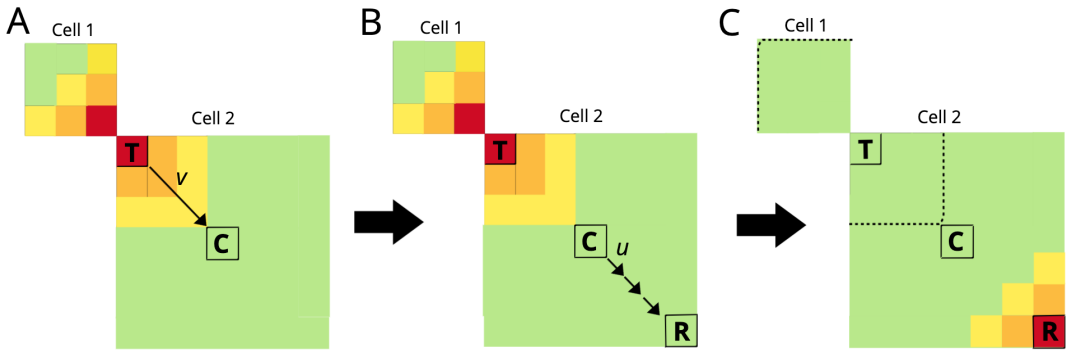

Figure 3.2: **Implementation of repolarisation**. A) Cell-cell contact occurs at site T. C represents the middle of the cell. The vector $\vec{v}$ from T to C is computed B) Finding the site opposite to C (termed R). The unit vector $\vec{u}$ of $\vec{v}$ is computed. The code goes from site C in steps of u, until the site at the edge of the cell is found. This site is termed R. C) The Act value around R is increased. The Act value of R is set to Max_{Act}. The Act value of sites around R is increased in proportion to their proximity to R.

Lastly, the occurrence of CIL is probabilistic in nature. The likelihood of a cell to undergo CIL increases when it makes contact with another cell at a site with a high actin concentration [17]. In our model, the probability of a cell to undergo CIL when its site T contacts another cell is expressed as $P = \frac{Act(T)}{P_{Max}}$, whereby P_{Max} is the probability of the cell undergoing CIL when $Act(T) = Max_{Act}$. Consequently, a cell is unlikely to undergo CIL when the contact occurs at its rear, where the Act value is zero.

Melanophore and Xanthophore Interactions

Xanthophores and melanophors undergo run-and-chase dynamics. When melanophores move away from xanthophores their movement is chiral; they move in an anticlockwise manner and thus repolarize not opposite of a contact site, but at a 90 degree angle of it. Upon contact of melanophores and xanthophores, the repolarisation site R is found by computing the vector $\vec{v}$ and its unit vector $\vec{u}$ in the same manner as described above (Fig. 3.3A). Then, the code performs steps of $\vec{u}$ from the cell centre C of the melanophores. Contrary to the method described before, the direction of the movement is at a 90 degree angle from the original contact site (Fig. 3.3B). When the site is found that is located on the cell edge, termed R, is found, then the change in Act value of the site and its neighbouring sites occurs in the same manner as described above. In the melanophore, protrusion inhibition is implemented as described before (Fig. 3.3B). Since xanthophores chase melanophores upon contact [13], the Act value of the contact site of the xanthophore is set to Max_{Act} (Fig. 3.3B).

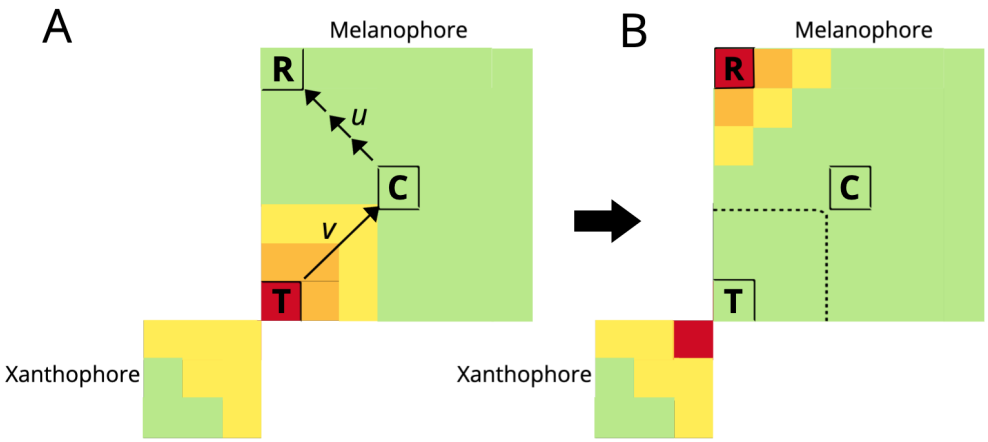

Figure 3.3: **Implementation of run-and-chase Dynamics between Melanophores and Xanthophores**. A) A melanophore contacts a xanthophore at a site T. The vector $\vec{v}$ from the centre of the melanophore (C) to the contact site T is computed. $\vec{u}$ denotes the unit vector of $\vec{v}$. From C, steps of $\vec{u}$ are performed at a 90 degree angle, until a site is found that is at the edge of the cell (termed R). B) Act values of the xanthophore and melanophores are modified. R obtains Act value Max_{Act}. The Act value of the sites neighbouring it is changed as described in the algorithm above. The Act value of site T is set 0. The Act value of all neighbours of degree $I_R - 1$ of T is also set to 0. The site at which the xanthophore contacts the melanophore receives Act value Max_{Act}.

3.2 Parameter search

Most parameters were taken from the Niculescu et al. paper on the Act model [8]. How other were found is described here.

3.2.1 Neural crest cells

Within our first results section, we aim to repicate biological results found from studying neural crest (NC) cells. Therefore, we aimed to find the values of Max_{Act} and λ_{Act} that enable our model to mimic NC migration, since these parameters greatly influence how our CIL implementation affects the cells. We first determined the values by looking at the speed of neural crest cells. NC cells show amoeboid-like cell movement [18], but move more slowly than amoeboid cells [19] [20]. In Niculescu et al. paper, for amoeboid cells the values $Max_{Act} = 20$ and $\lambda_{Act} = 200$. We decreased λ_{Act} to 120 for NC cells (to mimic their slower speed) and set $Max_{Act} = 30$.

In Niculescu's paper, $J_{cell,cell} = 100$ and $J_{cell,medium} = 20$. However, this leads to very low adhesion between cells. Therefore, we changed the values in order to mimic NC cell behaviour. In a CPM model of NC cells developed by Szabo et al., $J_{NC,NC} = 3$ and $J_{NC,medium} = 5$ [2]. Therefore, we mimiced the ratio of these values but increased the values of the things itself in order to fit our simulation better. Thus $J_{NC,NC} = 10$ and $J_{NC,medium} = 16$ were chosen.

3.2.2 Melanophores and xanthophores

Using FIJI, we analysed video data of melanophores and xanthophores from [9]. From this, we found that melanophores are on average four times bigger than xanthophores. Thus, the target area of xanthophores was set to 600 px^2 while that of melanophores was set to 150 px^2. The target perimeter of melanophores was set to 380 px, while that of xanthophores was set to 150 px. Melanophores move faster than xanthophores *in vitro* [9]. Therefore, $\lambda_{Act,M} = 200$ and $\lambda_{Act,X} = 120$ was chosen. Mathematical modeling has shown that xanthophores have a

higher adhesion strength between themselves that melanophores [21]. Therefore $J_{X,X} = 5.$ and $J_{M,M} = 10$ were chosen as parameters. $J_{M,X}$ was set to 16, to mimic the favourable adhesion between melanophores and xanthophores. All other parameters were replicated from above chosen set.

Chapter 4

Results: General mechanics

The parameters used for the simulation are described in Appendix A.

4.1 Two-cell simulations

Protrusion inhibition alone is not sufficient to replicate CIL behaviour. We first asked whether protrusion inhibition alone could accurately reproduce CIL behavior. To address this question, we performed simulations involving two cells on a one-dimensional grid, in order to mimic the setup of experiments performed by Scarpa et al. that looked at CIL behaviour in neural crest cells [19]. The one-dimensional array was modeled by setting the width of the grid to 150 and the height to 24. We kept the protrusion inhibition parameter (I_R) at a constant value of 1, with no incorporation of repolarisation. The parameter P_{Max} was set to two different configurations: a constant value of 1 (referred to as 'constant') and a dynamic value $\frac{Act(x)}{Max_{Act}}$ (referred to as 'linear'), where x represents the site touching a neighboring cell. The control group had $P_{Max} = 0$ and thus did not undergo CIL. It was assessed whether contact breaking and mean cell distance were different in each category. The criteria for "contact breaking" was determined as cells losing touch within 400 MCS of their initial contact. The mean distance was calculated by determining the average cell distance from the start of contact up to 500 MCS later.

Comparing the results of the two CIL implementations to simulations without CIL, we observed a significant difference in the mean cell distance between the groups (Fig. 4.1a). Specifically, the mean cell distance in the two CIL implementation groups was significantly lower than in simulations without CIL (P_{Max} = linear: 40.64 vs 36.11; $n = 20$; $p = 0.0055$; two-sample t-test. P_{Max} = constant: 41.52 vs 36.11; $n = 20, p = 0.0012$, two-sample t-test). Additionally, the contact breaking rate in the CIL implementation groups was significantly higher than in the group without CIL (Fig. 4.1b) (P_{Max} = linear: 0.85 vs 0.35, $n = 20$, $p = 3.94 \cdot 10^{-5}$, z-test for proportion. P_{Max} = constant: 0.90 vs 0.35, $n = 20, p = 9.305 \cdot 10^{-6}$, z-test for proportion). Thus, protrusion inhibition significantly alters cell dynamics.

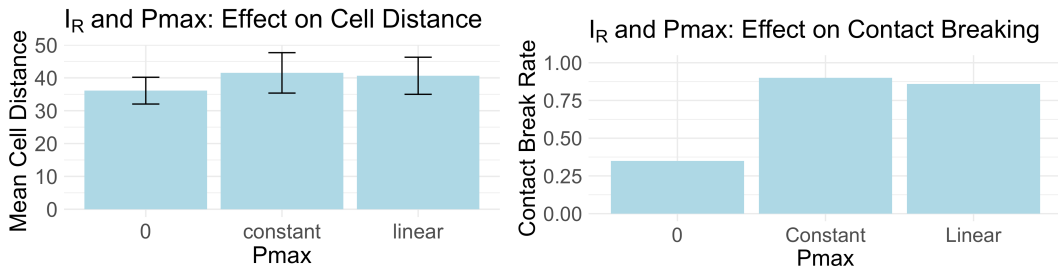

(a) Mean Cell Distance

(b) Contact breaking

Figure 4.1: **Impact of protrusion inhibition and repolarisation on mean cell distance and contact breaking.** a) Mean cell distance between nuclei from the point of initial contact until 500 MCS later, under various conditions: $P_{Max} = 0$ (no CIL),P_{Max} is linear and P_{Max} is constant ($P_{Max} = 1$), b) Percentage of time contact was broken during the 400 MCS observation window post initial cell-cell contact. Each condition was assessed over 20 independent runs.

Thus, is protrusion inhibition alone sufficient to mimic CIL dynamics? Not necessarily. In the study by Scarpa et al., it was observed that the mean distance between nuclei post-collision was approximately 1.25 times higher in cells undergoing CIL than in those that didn't undergo CIL. However, the mean cell distance in the constant and linear group was significantly less than 1.25 times that of the control group (P_{Max} = linear: mean = 40.64, $\mu = 45.14$, $n = 20$, $p = 0.0008$, z-test for proportion. P_{Max} = constant: mean = 41.52, $\mu = 45.14$, $n = 20, p = 0.0042$, one-tailed t -test). Thus, the increase in cell distance is not significantly large to mimic biological observations. Furthermore, when visually inspecting a time series of cell collisions with protrusion inhibition implemented, we observed that cells moved apart only slightly, without undergoing substantial changes in their direction of travel (Fig. 4.2). Cells transiently broke cell contact, but did not move far away from each other. These findings collectively indicate that protrusion inhibition alone is inadequate for replicating the dynamics of CIL.

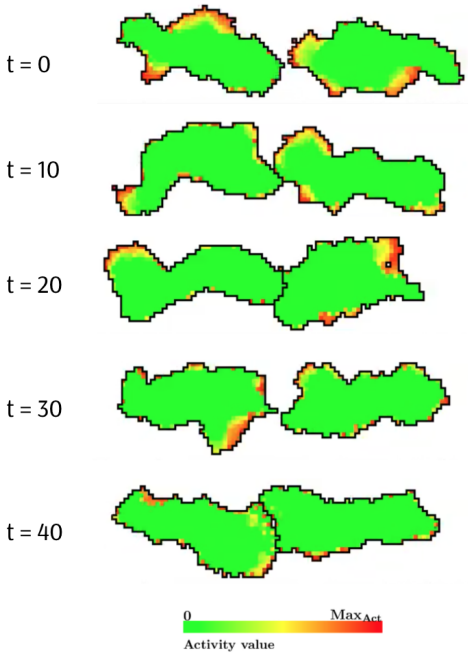

Figure 4.2: **Protrusion inhibition leads to transient breaking of cell-cell contacts**. A time series of the collision two cells in the CIL model. Colour within cells represents the Act value of the sites. Model was implemented was no repolarisation, $I_R = 1$, and $P_{Max} = 1$. Activity value bar adapted from [8].

Repolarisation prevents prolonged cell-contact when $P_{Max} = 1$. Subsequently, we introduced repolarisation into our model to investigate its effect on cell dynamics. Simulations were conducted with two configurations for I_R: 0 or 1, in combination with constant or linear P_{Max}. Additionally we included a control group where CIL was not implemented and P_{Max} was set to 0. The results are presented in Fig. 4.3a, which illustrates the mean cell distance, and Fig. 4.3b, which depicts the frequency of cell-contact breaking.

The incorporation of repolarisation significantly altered cell dynamics. For all combinations of I_R and P_{Max}, the mean cell distance and the contact breaking frequency significantly increased. Interestingly, mean cell distance was lower when $I_R = 1$ than when $I_R = 0$ for both conditions of P_{Max}, although these differences were not significant (P_{Max} = linear: 65.08 vs 60.30, $n = 20$, $p = 0.1443$, two-sample t-test. P_{Max} = constant: 66.27 vs 60.60 , $n = 20, p = 0.0871$, two-sample t-test). These results show that repolarisation increases mean cell distance and leads to more frequent contact breaking, regardless of whether protrusion inhibition is incorporated into the model.

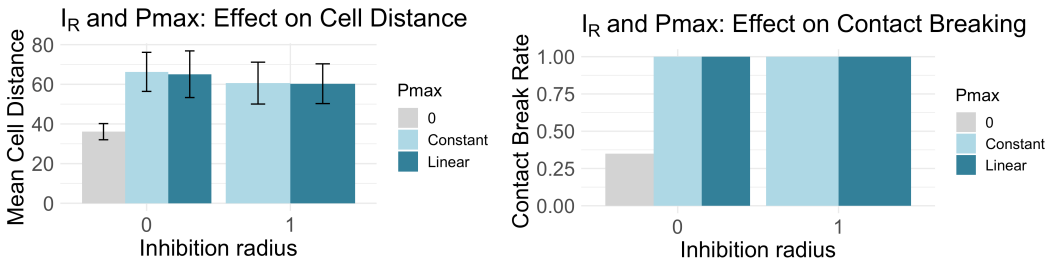

(a) Mean Cell Distance

(b) Contact breaking

Figure 4.3: **Impact of protrusion inhibition and repolarisation on mean cell distance and contact breaking.** a) Mean cell distance between nuclei from the point of initial contact until 500 MCS later, under various conditions values for I_R and P_{Max}. The control group, in which did not undergo CIL, is denoted in grey. b) Percentage of time contact was broken during the 400 MCS observation window post initial cell-cell contact Each condition was assessed over 20 independent runs.

The model did not perfectly replicate biological observations. Specifically, prior research by Scarpa et al. [19] reported that cells undergoing CIL exhibited a contact breaking rate ranging between 0.8 and 0.9, notably lower than the frequency of 1 observed in our simulations when repolarization was implemented (Fig. 4.3b). Furthermore, our observations during the simulation revealed that cells immediately moved away from each other upon contact, lacking the extended adherence period observed in biological settings (Fig. 4.4). This departure from the biological context, where cells remain in contact for some duration before undergoing repolarisation and subsequent separation, leads us to the conclude that, at $P_{Max} = 1$, our model exhibits an excessive tendency for cells to rapidly disengage upon contact, a phenomenon not in line with biological observations.

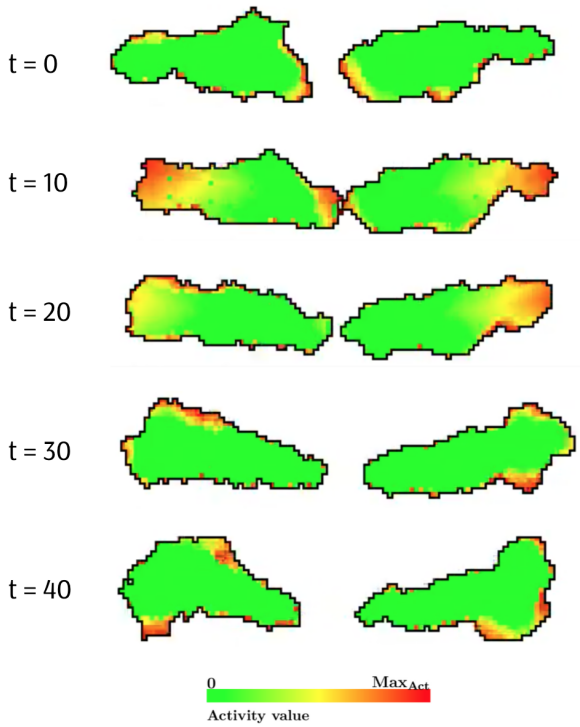

Figure 4.4: **Cells do not adhere when** $P_{Max} = 1$. A time series of the collision two cells in the CIL model. Colour within cells represents the Act value of the sites. Model was run with repolarisation, $I_R = 1$, and $P_{Max} = 1$. Activity value bar adapted from [8].

When $P_{Max} = 0.02$, repolarisation alone mimics CIL behaviour. We tried to address the problems of the last section by decreasing the value of P_{Max} to 0.02. We did this because we speculated that if CIL was less likely to occur, it would take some time for CIL to kick in, during which the cells could adhere to each other.

Fig. 4.5 presents several experimental conditions: absence of CIL ($I_R = 0$, Repolarisation = false), exclusive protrusion retraction ($I_R = 1$, Repolarisaton = false), only repolarisation ($I_R = 0$, Repolarisation = true), and a combination of both ($I_R = 1$, Repolarisation = true). It was assessed whether contact breaking and mean cell distance were different in each category.

The results show that the group with no CIL and the group with only protrusion inhibition had similar mean cell distances (36.11 px or 37.20 px, respectively; $p > 0.05$, $n = 20$, two-sample t-test) and similar times of lost contact (0.35 or 0.2, respectively, $p > 0.05$, $n = 20$, z-test for proportion). We also found that the group with only repolarisation and the group with both repolarisation and protrusion inhibition were similar in terms of mean cell distance (41.84 px or 44.55 px, respectively; $p > 0.05$, df=20, two-sample t-test) and lost contact times (0.75 or 0.8, respectively; $p > 0.05$, df = 20, z-test for proportion). However, all other comparisons between groups showed significant differences.

We find that for the group with repolarisation and $I_R = 1$, the mean cell distance is not significantly different from 1.25 times the mean distance of the group without CIL implemented (44.54 px and 45.14 px, $p = 0.72$, $n = 20$, two sample t-test). The same holds for the group with only repolarisation implemented (41.84 px and 45.14 px, $p = 0.055$, $n = 20$, two-sample t-test). Thus, we find that this group mimics biological observations.

Our results show that repolarisation by itself can mimic CIL behaviour, but protrusion inhibition on its own cannot. Additionally, our model shows that when $P_{Max} = 0.02$, the incorporation of repolarisation alone mimics CIL behaviour. Therefore, this model is used for subsequent studies.

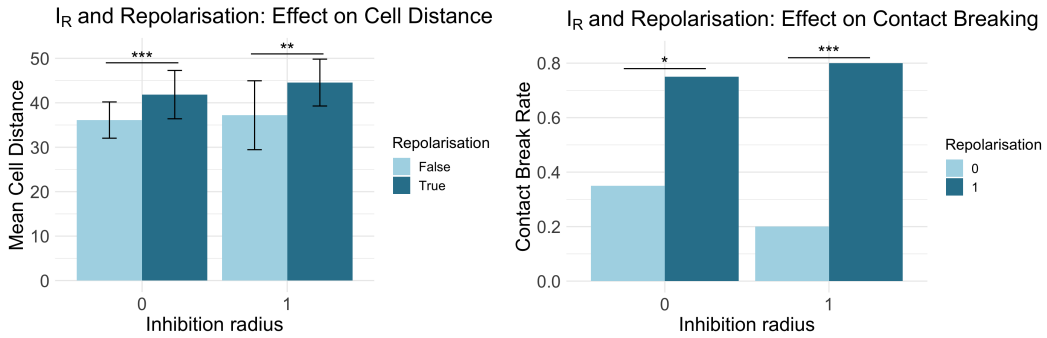

(a) Mean Cell Distance

(b) Contact breaking

Figure 4.5: **Impact of protrusion inhibition and repolarisation on mean cell distance and contact breaking.** a) Mean cell distance between nuclei from the point of initial contact until 500 MCS later, under various conditions: no CIL, only protrusion retraction ($I_R = 1$), only repolarisation ($I_R = 0$), and the combined effect of both components ($I_R = 1$, Repolarisation = TRUE). b) Percentage of time contact was broken during the 400 MCS observation window post initial cell-cell contact. Patterns of significance mirrored those observed for mean cell distance. Each condition was assessed over 20 independent runs.

A visualisation of the model is given by in Fig. 4.6. It is visible that the cells upon collision transiently maintain cell contact, before repolarising in opposite directions and moving away. At $t = 30$, the cells make contact. At $t = 40$, protrusion inhibition occurs, leading to low act value at the collision sites. At the same time, repolarisation leads to an increase in Act values on the rear side of the cells. At $t = 50$, the cells have clearly repolarised, which leads to cells moving away from each other. At $t = 70$, cells are still in contact due to cell adhesions, which are broken at $t = 80$.

Cell distance transiently increases after cell-cell contact. Next we asked how cell-cell contact affects cell distance. We simulated two cells with CIL implementation. Fig. 4.7 shows

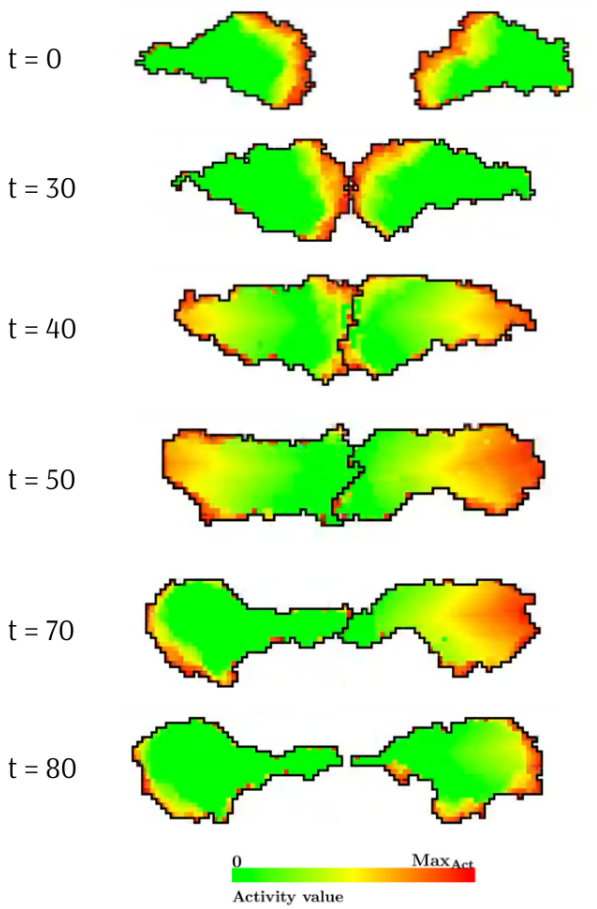

Figure 4.6: **Cell contact results in cells changing their direction of movement.** A time series of the collision two cells in the CIL model. Activity value bar adapted from [8].

the distance between the cells over time. The red dots denote timepoints at which cell-cell contact was made. After cell-cell contact is made, cell distance decreases slightly, followed by a significant increase in distance. The initial decrease most likely occurs because the CIL mechanism is probabilistic. Thus, it takes time for the mechanism to be initiated and for the cells to become repulsed. Then, cell distance increases again, until cells start to move in random directions and make contact again, repeating the cycle.

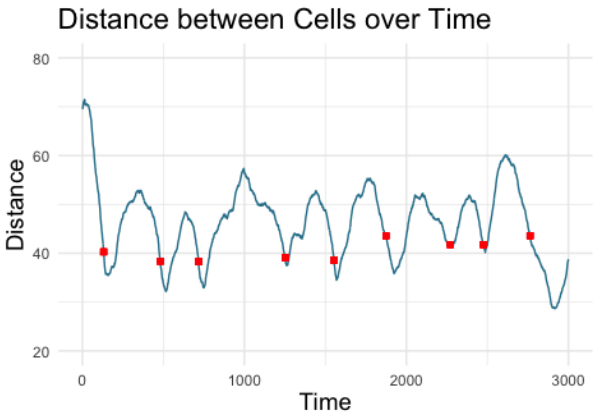

Figure 4.7: **Cell contact leads to a transient decrease in cell distance, followed by an increase.** A time series of the distance between two cells. Red dots denote moments of cell collision.

Increased CIL probability leads to more contact inhibition; Varying the inhibition radius has no significant effect. Next, we investigated the effect of wider range of possible values of I_R and P_{Max}. We varied I_R between 0, 1, 5, and 10, and P_{Max} between $0.001, 0.002$, and 0.005 and measured the effect on the mean cell distance post-collision and the contact breaking rate.

Fig. 4.8, top shows the effect of these parameters on mean cell distance. Surprisingly, varying the inhibition radius did not have a significant effect on the average cell distance for any value of P_{Max} (ANOVA, $p > 0.05$ for all values of P_{Max}). Increasing P_{Max} did lead to increased average cell distance. The same pattern can be observed for the percentage of time that contact was broken among cells (Fig. 4.8, bottom). Again, varying the inhibition radius did not significantly alter the contact breaking rate for any value of P_{Max} (Chi square test, $p > 0.05$ for all values of P_{Max}). These results confirm that, when P_{Max} is sufficiently small, protrusion retraction has a minimal effect on cell interactions and that the main effect is dictated by repolarisation.

Varying P_{Max}, however, did have a significant effect on the mean cell distance and contact breaking rate. Regarding the mean distance, for all values of I_R, there was no significant difference in the mean distance when $P_{Max} = 0.001$ and $P_{Max} = 0.002$ (two-sample t-test). There was a significant difference in the mean distance $P_{Max} = 0.001$ and $P_{Max} = 0.002$ for all values of I_R except for $I_R = 5$. When I_R, the difference in the mean distance was significant between $P_{Max} = 0.001$ and $P_{Max} = 0.005$ ($41.86\ px$ and $50.26\ px$, respectively, $p = 0.001$, $n = 20$, two-sample t-test). Thus, an increased value P_{Max} leads to a larger cell distance post-collision.

Regarding the contact breaking frequency, for all values of I_R, the difference between the contact breaking rate when $P_{Max} = 0.001$ and $P_{Max} = 0.005$ was significant (two-proportion z-test). Thus increased P_{Max} leads to more frequent contact breaking between cells.

From this we may conclude that P_{Max}, but not I_R, significantly influences the mean cell distance and contact breaking rate.

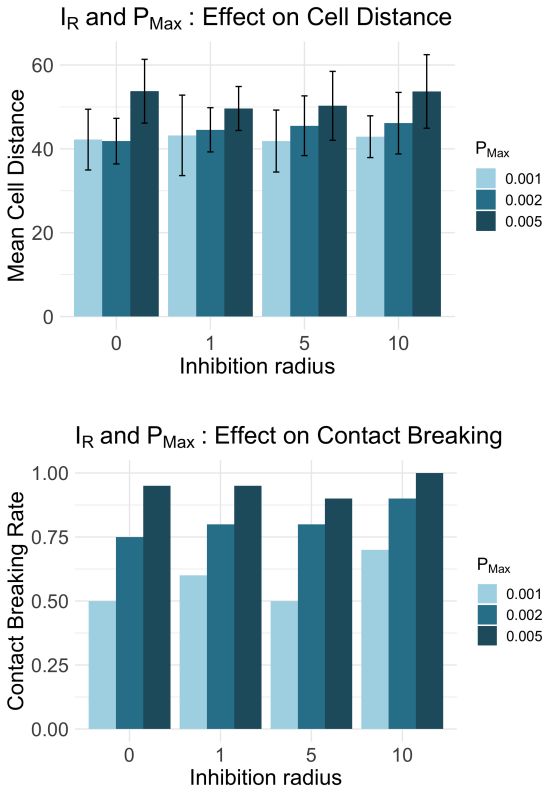

Figure 4.8: **Impact of Protrusion Inhibition and Probability of CIL occurring on mean Cell Distance and Contact Breaking.** Top) Mean cell distance between nuclei from the point of initial contact until 500 MCS later, under various conditions. Inhibition radius was varied between 0, 1, 5, and 10. The maximum probability of CIL occuring P_{Max} was varied between 0.001, 0.002, and 0.005. Bottom) Percentage of time contact was broken during the 400 MCS observation window post initial cell-cell contact. Conditions were varied in the same way as in the upper figure. Each condition was assessed over 20 independent runs.

4.2 Cell cluster simulations

Having shown that our CIL simulation obtains biologically significant results in a two-cell scenario, we turn to cell cluster simulations to observe whether we are able to simulate simple patterns.

CIL implementation induces radial dispersion in cell clusters. Scarpa et al. demonstrated that while migratory NC (mig-NC) cells, which undergo CIL, tend to disperse from circular clusters, premigratory NC (premig-NC) cells, lacking CIL, remain relatively clustered [22]. In our simulation, a cluster of $n = 10$ cells was considered. For the mig-NC cluster, parameters from the previous section were adopted. To model the cohesive nature of premig-NC cells, we set the cell-cell adhesion strength to $J_{premig-NC,premig-NC} = 4$, reflecting their stable cell-cell junctions, unlike the mig-NC cells [22]. This difference in behaviour is also supported by the higher concentration of adhesion proteins α-catenin and β-catenin at premig-NC junctions [22].

To isolate the effect of CIL from mere adhesive strength differences, we also introduced CIL in a simulated premig-NC cluster. Fig. 4.9A visualizes the temporal progression of these clusters. Noticeably, the premig-NC cluster without CIL remains mostly intact, except for a few cells that drift. In contrast, clusters of both premig-NC with CIL and mig-NC exhibit pronounced dispersion. Fig. 4.9B quantifies this by measuring the average inter-cellular distance from 100 to 3000 MCS. At $t = 3000$ MCS premig-NC cells without CIL have a significantly smaller mean

intercellular distance than their CIL-equipped counterparts (mean inter-cellular distance: 51.4 and 86.6, respectively; $p < 0.05$, $n = 5$, two-sample t-test) and mig-NC cells (mean inter-cellular distance: 51.4 and 84.7 , respectively; $p < 0.05$, $n= 5$, two-sample t-test). This shows that CIL induces dispersion of cell clusters.

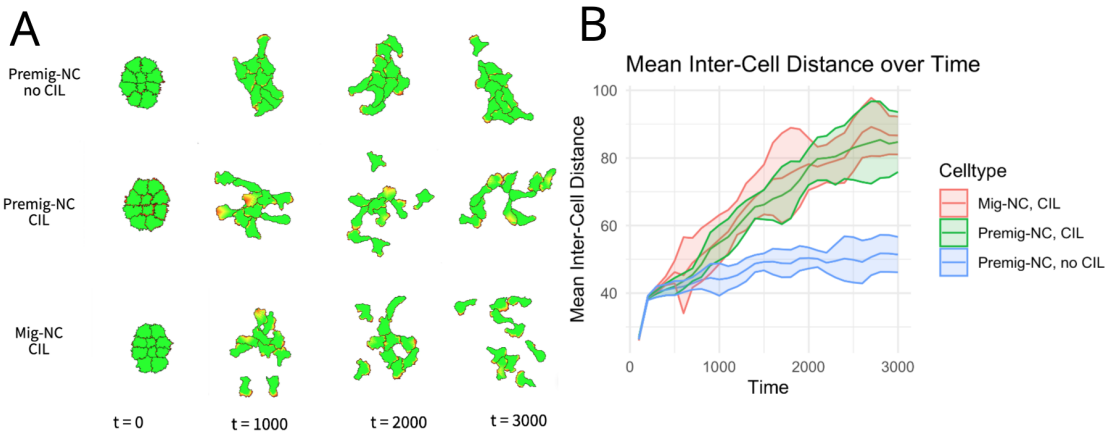

Figure 4.9: **CIL induces dispersion in cell clusters.** A) Temporal visualization of cell cluster dispersion for premig-NC without CIL (top), premig-NC with CIL (middle), and mig-NC with CIL (bottom). The absence of CIL in premig-NC results in minimal scattering at t = 3000 MCS, while CIL presence enhances scattering. B) Average intercellular distance from 100 to 3000 MCS. The data, sourced from 5 simulation runs, shows the minimal dispersion in premig-NC clusters without CIL as opposed to those with CIL.

CIL Implementation does not mimic haemocytes dispersion in *Drosophila*. In the course of *Drosophila* development, haemocytes exhibit a particular pattern of dispersion. Initially aligning along the midline, these cells subsequently disperse to form a three-line pattern, as illustrated in Fig. 4.10. This phenomenon is primarily driven by CIL interactions between the cells. Our aim to evaluate whether our model could replicate this behaviour. Given the small, rounded morphology of haemocytes, we set the target area to $400\,px^2$ and the target perimeter to $250\,px$. As haemocytes move more slowly than NC cells, λ_{Act} was reduced to 90 [19][3]. Furthermore, the cell-cell adhesion parameter, $J_{H,H}$, was set to 20.

We initiated the simulation with $n = 30$ cells aligned in a straight line, consistent with the cell count used in a previous study by Davis et al. [3]. Fig. 4.11 presents a time series depicting haemocyte movement. Contrary to the expected three-line arrangement, our model produced a random spatial distribution, with some instances of cell clustering.

What could be the underlying cause for this discrepancy? We hypothesize that the mechanism of CIL in haemocytes differs from that in NC cells. Specifically, NC cells experience CIL upon direct body contact, whereas haemocytes undergo repulsion via lamellae extensions even when separated (see Fig. 4.12). This mechanism allows each haemocyte to maintain a unique spatial niche, repelling other cells that venture into this territory through lamellae-mediated contact. To incorporate this aspect into our model, a CPM extension accounting for lamellae is necessary, a topic we delve into in the Discussion section.

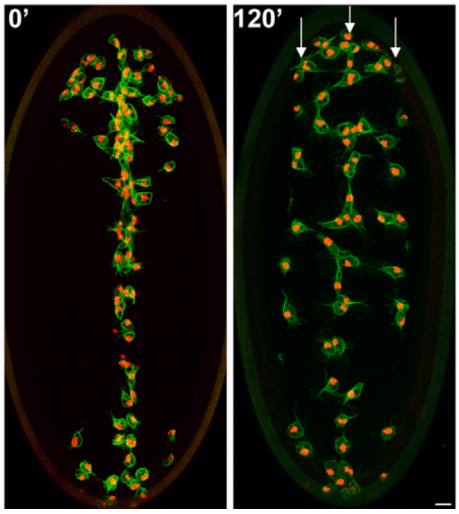

Figure 4.10: **CIL Induces Dispersion in *Drosophila* haemocytes.** An *in vivo* representation of haemocyte dispersion in *Drosophila*. At 0' a one-line pattern is observed. Due to CIL, over time a three-line pattern emerges. Adapted from [3].

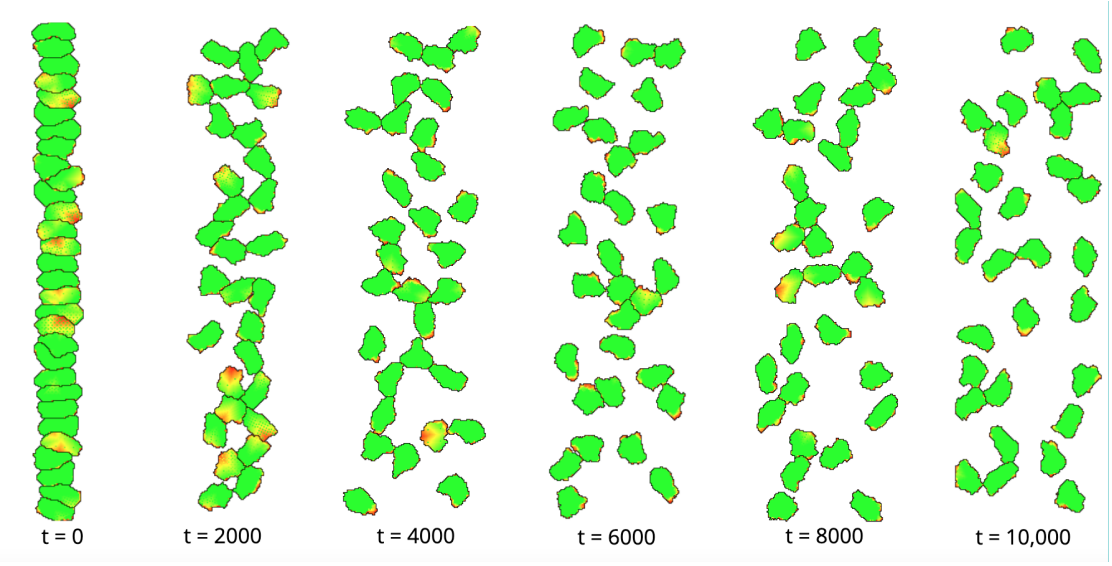

Figure 4.11: **CIL implementation does not lead to three-stripe pattern.** A time series of the distribution of haemocytes. At $t = 0$, the haemocytes are positioned in a line to mimic the initial distribution of haemocytes in *Drosophila*. By $t = 10,000$ the cells have dispersed. but the configuration is random and not in a three-line pattern.

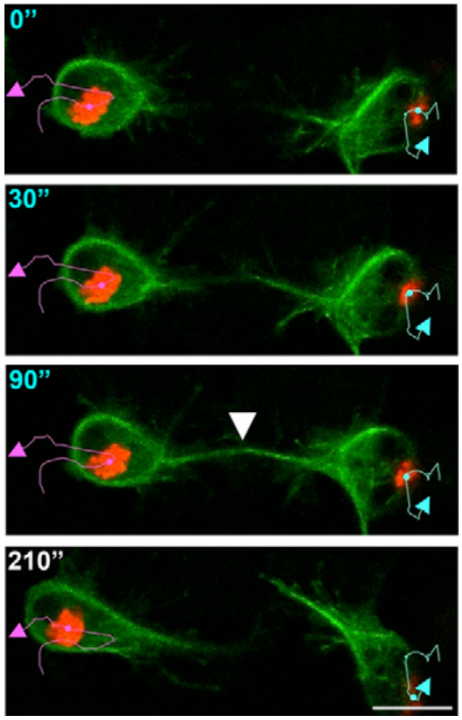

Figure 4.12: **Contact of lamellae leads to CIL in *Drosophila* haemocytes.** A time series of the interaction of *Drosophila* haemocytes. Cells are denoted in green and their nuclei in red. The arrow shows the point at which the lamellae of the cells touch. Adapted from [3].

Chapter 5

Results: Zebrafish stripe formation

Having explored the general dynamics of our model, we now implement it to explore melanophore and xanthophore interactions.

5.1 Behaviour of systems with two cells

Run-and-chase behaviour does not arise when CIL is not implemented. Our aim in this section was to see whether chiral run-and-chase behaviour could be replicated in our model. We first verified that run-and-chase dynamics do not arise spontaneously without CIL implementation. We simulated a melanophore and xanthophore on a one-dimensional lattice without CIL implementation and without active movement of the xanthophore towards the melanophore. This pair was termed the X_{KO}, M_{KO} pair. The relative location of the xanthophore and melanophore 100 MCS after collision was recorded. Fig. 5.1A shows the frequency of relative location of the xanthophore and melanophore post-collision, as observed *in vitro* by Kondo et al. Fig. 5.1B shows the result of our simulations with the X_{KO}, M_{KO} pair. As is visible, the distribution of the angles differs for the two plots, indicating that cell behaviour is not replicated.

We then asked whether incorporating active movement of xanthophores towards melanophores could be sufficient to mimic run-and-chase behaviour. Thus, when xanthophores made contact with melanophores, the Act-value at their contact site was set to Max_{Act}. This pair was termed the X, M_{KO} pair. Fig. 5.1C shows the relative movement of these cells, simulated in the same conditions as the previous pair. It is visible that movement of the cells again does not correspond to the experimentally observed movements. Again, the xanthophore and melanophore movement does not mimic experimental results.

Thus, we conclude that run-and-chase movement does not occur when CIL is not implemented in melanophores.

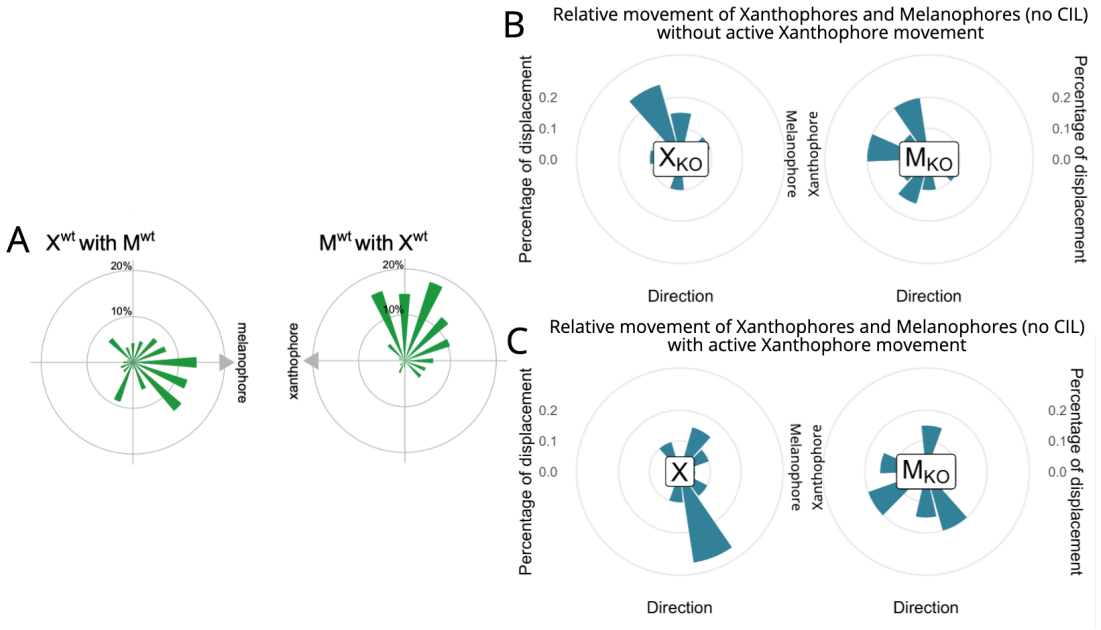

Figure 5.1: **Xanthophore and Melanophore simulations do not mimic run-and-chase behaviour when CIL is not implemented how chiral movement.** A) Relative movement of xanthohores and melanophores *in vitro*, as observed by Yamanaka and Kondo [9]. Xanthophores move towards melanophores at an angle between 0 and 45 degrees, while melanophores move away at an angle between 60 and 140 degrees. Adapted from [9]. B) Result of simulations between xanthophore and melanophore interactions, without active movement of xanthohores towards melanophores and without CIL implementation in melanophores. The movements are shown relative to the other celltype. C) Result of simulations between xanthophore and melanophore interactions, with active movement of xanthophores towards melanophores and without CIL implementation in melanophores. The movements are shown relative to the other celltype. Twenty runs were assessed.

Run-and-chase behaviour is not replicated when melanophores repolarise opposite to the contact site. Having concluded that run-and-chase dynamics do not occur when melanophores do not undergo CIL, we included CIL as described in the previous section. Thus, melanophores repolarise opposite to the contact site upon contact with xanthophores.

Fig. 5.2 shows the relative movement of the cells, without active xanthophore movement (Fig. 5.2B) and with active xanthophore movement (Fig. 5.2C). We can observe that experimental patterns are not mimicked in these simulations.

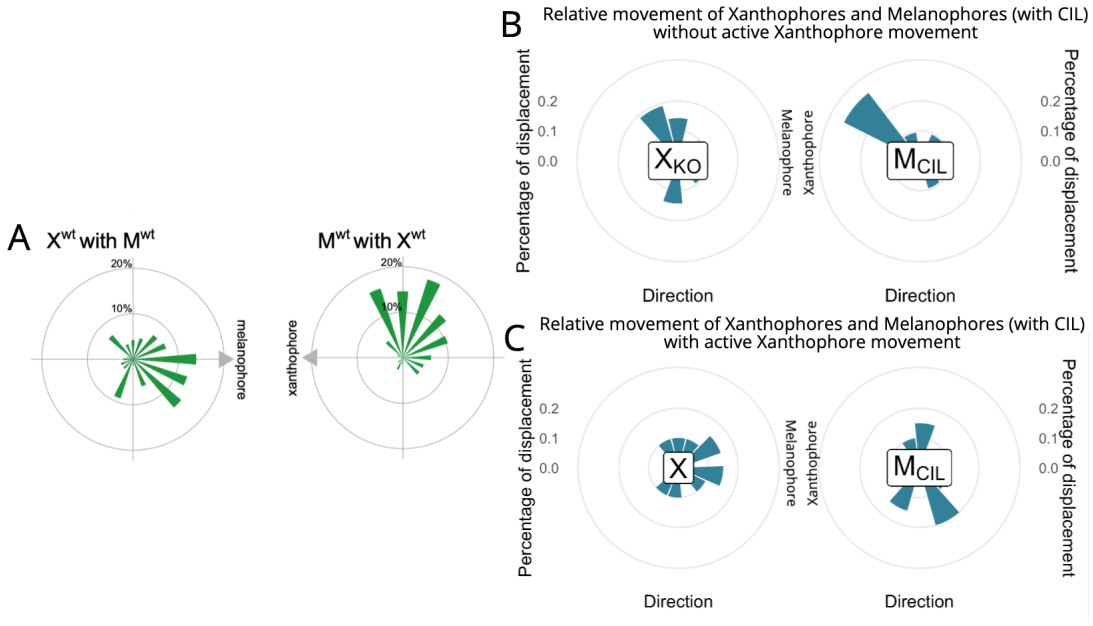

Figure 5.2: **Xanthophore and Melanophore simulations do not mimic run-and-chase behaviour when melanophore repolarisation occurs opposite to the contact-site** A) Relative movement of xanthohores and melanophores *in vitro*, as observed by Yamanaka and Kondo [9]. Xanthophores move towards melanophores at an angle between 0 and 45 degrees, while melanophores move away at an angle between 60 and 140 degrees. Adapted from [9]. B) Result of simulations between xanthophore and melanophore interactions, without active movement of xanthohores towards melanophores and with CIL implementation melanophores. The movements are shown relative to the other celltype. C) Result of simulations between xanthophore and melanophore interactions, with active movement of xanthophores towards melanophores and with CIL implementation in melanophores. The movements are shown relative to the other celltype. Twenty runs were assessed.

Fig. 5.3 shows a time series of the xanthophore-melanophore interaction in this movement. Experiments have shown that melanophores circle around xanthophores in a counter-clockwise manner. In Fig. 5.3 we observe, however, that melanophores simply move away from xanthophores and do not circle them. Thus, these dynamics do not mimic experimental observations.

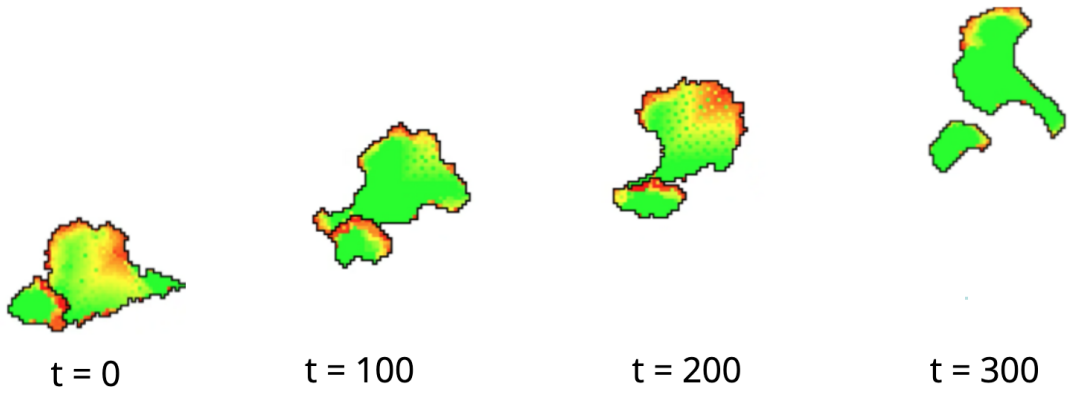

Figure 5.3: **Melanophores outrun Xanthophores when repolarisation is chiral.** A time series of xanthophore and melanophore interactions. Xanthophores were implemented to actively move towards melanophores, while melanophores repolarise opposite to the contact site.

Overall, the lack of chiral cell movement between the cells leads us to conclude that this implementation is insufficient to mimic chiral run-and-chase behaviour.

When melanophore repolarisation occurs at a 90 degree angle, chiral run-and-chase dynamics are replicated. To mimic the chiral movement, we implemented the previously described model, but amended it so that melanophore repolarisation would not occur opposite of the contact site (at 180 degrees), but at 90 degrees (as described in the Methods section). Fig. 5.4B and C show the relative movement of xanthophores and melanophores 100 MCS after collision. As is visible, our model replicates the results of Kondo and Yamanaka, regardless of whether active movement is implemented (Fig. 5.4B).

Next, we verified that run-and-chase dynamics do not differ significantly regardless of whether active movement of xanthophores is implemented. We did this by comparing the proportion of xanthophore movements that occur between 0 and 45 degrees and the proportion of melanophore movements that occur between 60 and 140 degrees in the two cell pairs (Fig. 5.5). Although the proportion is lower for the knockout pair, the difference is not statistically significant. Thus, active movement of xanthophores towards melanophores is not necessary to mimic xanthophore-melanophore dynamics. In further simulations, the active movement is not included.

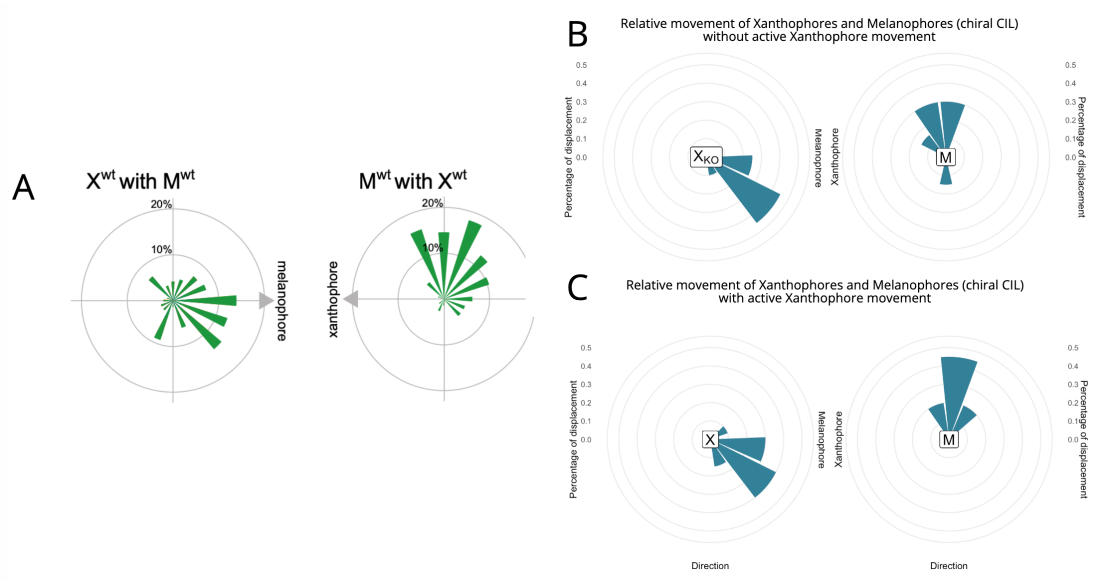

Figure 5.4: **Xanthophores and Melanophores show chiral movement.** A) Relative movement of xanthohores and melanophores *in vitro*. Xanthophores move towards melanophores at an angle between 0 and 45 degrees, while melanophores move away at an angle between 60 and 140 degrees. Adapted from [9]. B) Result of simulations between xanthophore and melanophore interactions, whereby active movement of xanthophores was not implemented. Melanophores repolarised at 90 degrees upon xanthophore contact. Movement mimics that observed experimentally. C) Result of simulations of the interaction between xanthophore an melanophores, with active movement of xanthophores implemented. Melanophores repolarised at 90 degrees upon xanthophore contact

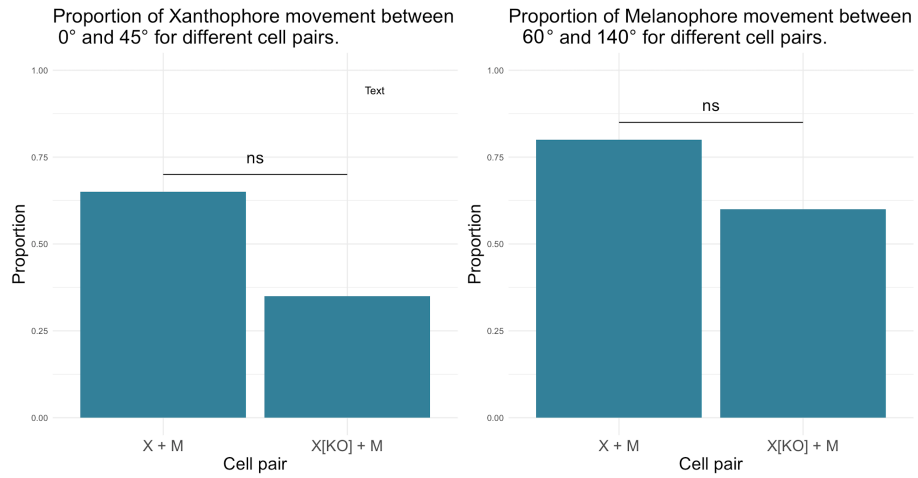

Figure 5.5: **Experimental observations are replicated without active movement of xanthophores towards melanophores.** Bar chart showing the proportion of xanthophore (left) and melanophore (right) movement in experimentally observed angles for the X, M and X_{KO}, M pair. The difference in between the pairs is not significant ($p > 0.05$).

Fig. 5.6 shows a step-by-step progression of the model. Upon contact of the melanophore with the xanthophore, the melanophore repolarises chirally. Due to high melanophore-xanthophore adhesion, it is not able to break away from the xanthophore. Thus, its repolarisation continues, leading to it spiraling in an anti-clockwise manner around the xanthophore. These dynamics are in line with experimental results.

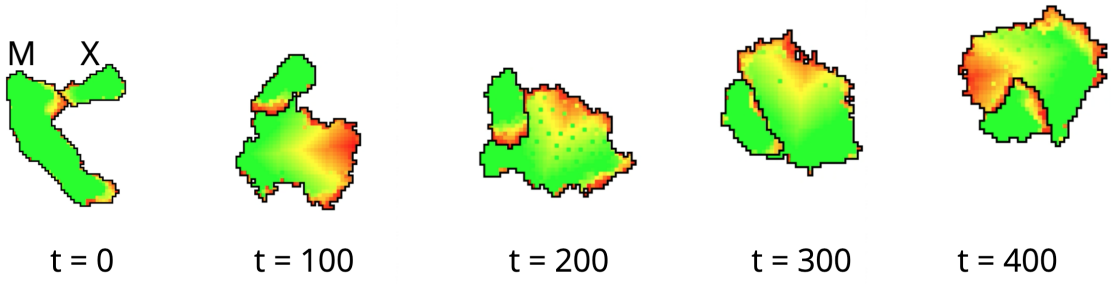

Figure 5.6: **Melanophore-xanthophore interaction leads to chiral movement of both cells.** A time series of a melanophore-xanthophore interaction. The melanophore is denoted by M, while the xanthophore is denoted by X.

Overall, our model model replicates melanophore and xanthophore dynamics. It should be noted that although chiral movement of melanophores was included in our model, that of xanthophores was not. Therefore, the chiral movement of xanthophores observed in our results is an emergent phenomenon.

5.2 Stripe patterns

Having verified that our model mimics two-cell behaviour, we turn to zebrafish patterns. The first question we aim to answer is whether run-and-chase dynamics could occur *in vivo*. Though run-and-chase occurs between melanophores and xanthophores *in vitro*, its role in stripe pattern formation is contested. Woolley et al. has argued that run-and-chase behaviour alone is not sufficient to explain pattern development [12]. They created a mathematical model mimicking the experimental observations of Kondo and Yamanaka and observed that the pattern was not stable. Since stable patterns are a prerequisite for pattern formation, they concluded that run-and-chase behaviour could not explain zebrafish pattern formation. However, in their model

they looked at a random initial distribution of cells and thus could only show that in a random distribution of cells the dynamics are unstable. Therefore, here we implement our model with the initial distribution of zebrafish stripes, to see whether these are stable when run-and-chase interactions occur.

The second question we aim to answer is the function of the chiral movement observed in melanophores and xanthophores. Kondo and Yamanaka proposed that the role of this chiral movement is to stabilize patterns [13], since the unidirectional movement of melanophores prevents melanophore clashing and thus prevents stripe intermingling (Fig. 5.7.) We use our model in order to observe in which cases chiral movement uniquely leads to stable patterns and what the prerequisites for this stability are.

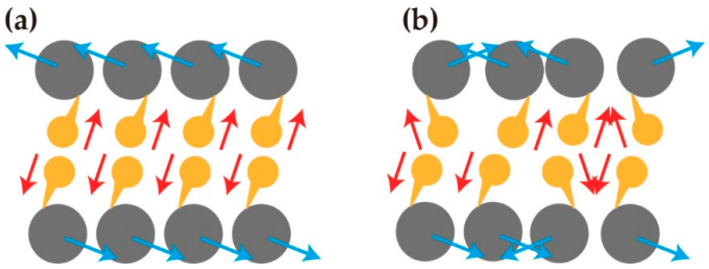

Figure 5.7: **Model image of the role of chirality in melanophore and xanthophore interaction** a) When chiral movement of melanophores occurs, all melanophores move in one direction. b) When the movement of melanophores and xanthophores occurs in random direction, clashing occurs between the cells. Adapted from [13].

Run-and-chase behaviour does not lead to stable patterns under random initial cell distributions. First we aimed to verify that our run-and-chase model mimics the findings of Woolley et al., namely that under a random initial distribution of melanophore and xanthophores, no stable pattern is formed. We simulated twenty melanophores (grey) and xanthophore (yellow) randomly distributed in a 150 by 150 grid (Fig. 5.8). Fig. 5.8A shows the distribution of the cells over time. Over time, dispersal of cells occurs and no stable pattern is observed. Fig. 5.8B shows the mean inter-cell distance over time. The mean inter-cell distance increases over time. If the pattern was stable, we would expect the mean inter-cell distance to stay the same. However, there is a significant difference between the mean distance at $t = 100$ and $t = 3000$ (7786 and 17761, respectively; $p < 0.05$, $n = 10$, two-sample t-test). Overall, our results are in agreement with those of Woolley et al.

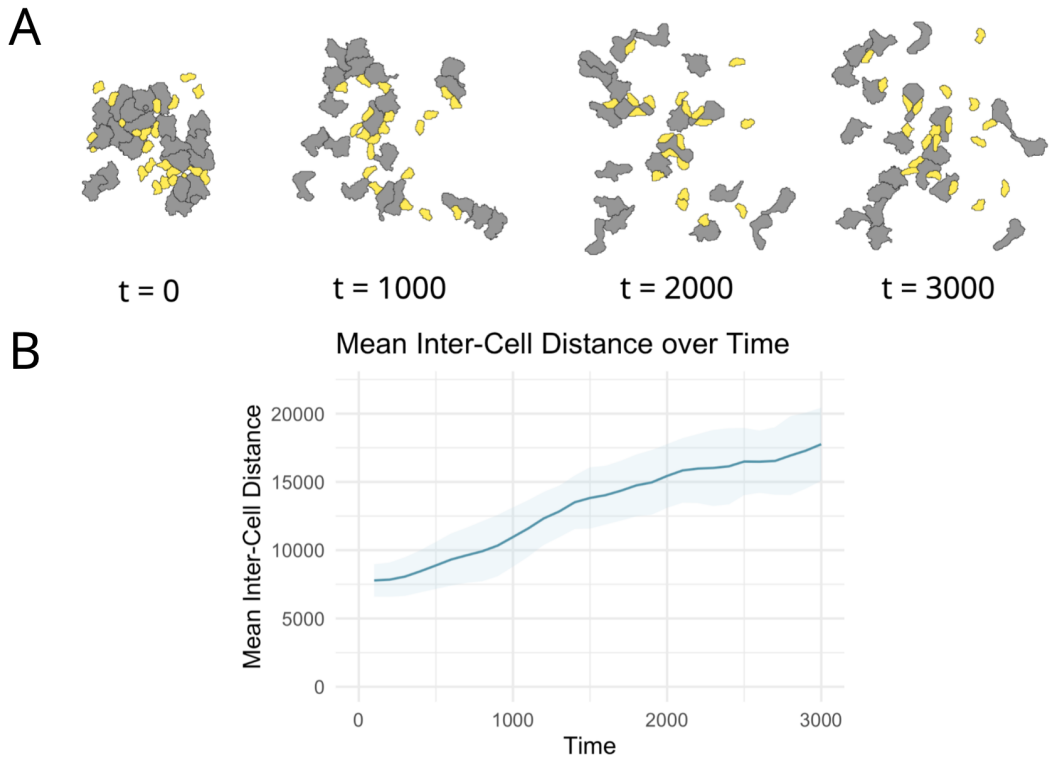

Figure 5.8: **Cell Dispersal occurs under Run-and-Chase Dynamics.** A) A time series of a simulation with twenty melanophores and xanthophores with a random initial distribution. Grey cells denote melanophores, while yellow cells denote xanthophores. Run-and-chase dynamics were implemented between melanophores and xanthophores. B) Mean inter-cell distance plotted over time. The blue area denotes the standard deviation. Ten runs were performed.

Run-and-chase behaviour leads to unstable zebrafish patterns. We implemented our model in zebrafish stripe simulation with three xanthophore stripes and two melanophore stripes (Fig. 5.9A and B). The xanthophores are shown in yellow, in order to differentiate them from the melanophores, whose colour depends on the Act values their sites posses (red: $Act(x) = Max_{Act}$, green: $Act(x) = 0$). The number of cells was 128, of which 40 melanophores and 88 xanthophores. Stripe 1 (top) and 5 (bottom) were two cells wide, while the inner stripe were modelled to be four cells wide, based on observations from a zebrafish study by Takahashi and Kondo [23]. Run-and-chase dynamics were implemented as described in the section above, whereby active movement of xanthophores towards melanophores was not implemented. The model was implemented with periodic boundaries, in order to simulate the presence of a larger patterns. Fig. 5.9A shows a time series of the stripe. As is visible, by $t = 1000$, the stripes already become crooked. By $t = 3000$, the inner xanthophore stripe has become a cluster and strong intermixing of xanthophore and melanophore has occured. Thus, under these conditions, the stripe pattern is not stable.

We asked whether this may be caused by the periodic boundaries and ran simulations without them (Fig. 5.9B). A similar pattern occurred, whereby by $t = 1000$, the inner xanthophore stripe lost its straightness and by $t = 3000$, the two melanophore stripes had intermixed. Thus, the implementation of the experimentally observed interactions between xanthophores and melanophores leads to unstable pattern formation, regardless of boundary conditions. We verified this by calculating the mean number of cells touching cells of non-adjacent stripes at $t = 3000$ (Fig. 5.9C). If the stripe pattern was stable, we'd expect this number to be zero. For both conditions, the mean is statistically greater than 0 (periodic boundaries = false: $p < 0.001$, periodic boundaries = true: $p < 0.005$), indicating that the pattern is unstable.

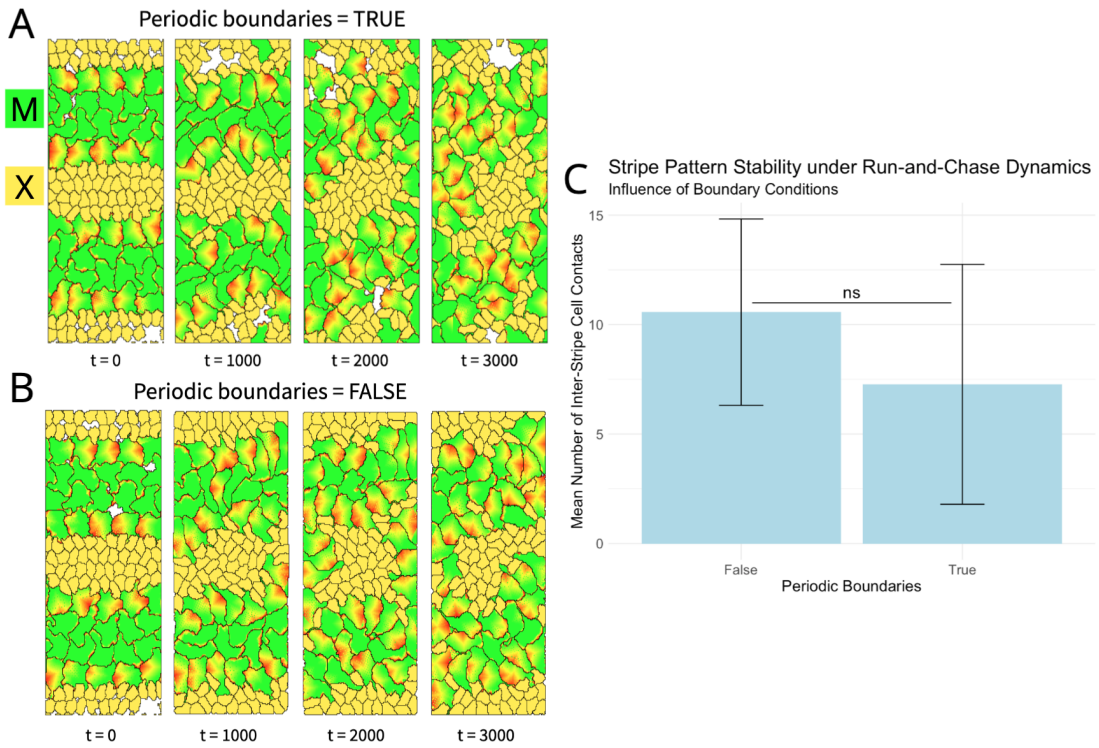

Figure 5.9: **Run-and-Chase movements lead to stripe pattern instability.** A) A time series of the stripe pattern simulation with three xanthophore stripes (yellow) and two melanophore stripes (green) with periodic boundary implementation. Over time, the stripes lose their straightness and cells from one stripe start mixing with cell of non-adjacent stripes. B) A time series of a simulation with the same pattern, but without periodic boundaries. Over time, similar movement is observed as in A). C) Barchart denoting the number of cells having contact with cells of non-adjacent stripes at $t = 3000$. Regardless of whether periodic boundaries are implemented, the mean is greater than 0, indicating that stripe intermixing occurs.

What may be the cause of this? We hypothesized that this occurs because movement of xanthophores towards melanophores leads to xanthophores breaking away from their stripe and moving into the melanophore stripe. To test this hypothesis, $\lambda_{Act,Xanthophore}$ was set to 1 in order to lower the speed of xanthophores. Fig. 5.10A and B show a time series of the stripes with this implementation. As is visible, both when periodic boundaries are (Fig. 5.10A) and are not (Fig. 5.10B) implemented stripe intermixing occurs less than when $\lambda_{Act,xanthophore} = 160$. This was quantified in Fig. 5.10C, which shows the proportion of cells touching cells at non-adjacent stripes at $t = 3000$. When $\lambda_{Act,xanthophore} = 1$, this number is not significantly different from 0 (periodic boundaries = false: $p \gg 0.05$). Thus, stripe intermixing occurs less when $\lambda_{Act,xanthophore} = 1$. This, however, does not indicate that the pattern is stable, since the inner stripe show crookedness by $t = 3000$. For stripes 2-4, the mean square distance (MSD) of the cells to their stripe axis was measured at $t = 150$ and $t = 3000$ for $\lambda_{Act,xanthophore} = 160$ and $\lambda_{Act,xanthophore} = 1$ and with or without periodic boundary implementation (Fig. 5.11). Under all four different conditions the MSD was significantly higher at $t = 3000$ than $t = 150$, indicating that the cells had moved away from their stripes. The strongest effect was seen when $\lambda_{Act,xanthophore} = 160$ and periodic boundaries were not implemented. From this, we conclude that even when xanthophores show slow movement, due to the fact that melanophores undergo CIL, stripe dynamics are unstable.

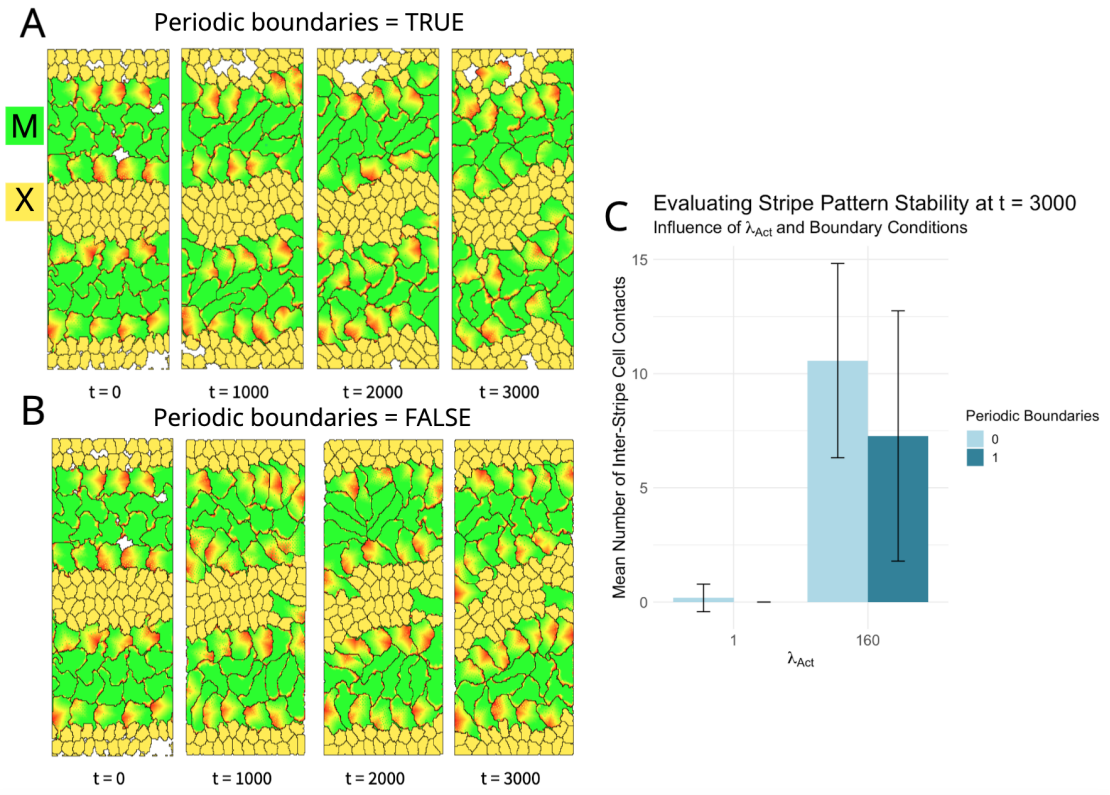

Figure 5.10: **Run-and-Chase dynamics with slow xanthophore movements lead to stripe pattern instability.** A) A time series of the stripe pattern simulation with three xanthophore stripes (yellow) and two melanophore stripes (green) with periodic boundary implementation. $\lambda_{Act,xanthophore}$ was set to 0 to simulate slow xanthophore movement. Over time, the stripes loose their straightness and cells from one stripe start mixing with cell of non-adjacent stripes. B) A time series of a simulation with the same pattern, but without periodic boundaries. Over time, similar movement is observed as in A). C) Barchart denoting the number of cells having contact with cells of non-adjacent stripes at $t = 3000$, when $\lambda_{Act} = 1$ and $\lambda_{Act} = 160$. Regardless of whether periodic boundaries are implemented, when $\lambda_{Act} = 1$ the mean is not significantly different from 0, indicating that stripe intermixing does not occur.

Chiral melanophore movement leads to the clockwise circulation of cells. Does this mean that chiral movement does not play a role in pattern formation? Not necessarily. We studied the effect that chiral movement has on a simpler pattern. We simplified the pattern from the previous simulation by looking at only two xanthophore stripes and one melanophore stripe, without periodic boundaries. This way, cells were confined to a smaller space. $\lambda_{Act,xanthophore}$ was set to 1 in order to preventing xanthophore dispersal. Fig. 5.14 shows a time-series of cellular movement. It can be observed that the melanophores circle around their stripe in a clockwise manner. Melanophores within the stripe (that do not touch xanthophores) stay confined there, whilst melanophores on the periphery of the stripe are pushed forward due to their repolarisation and the movement of their neighbours. Circulation occurs even though no xanthophores are present on the left and right edge.

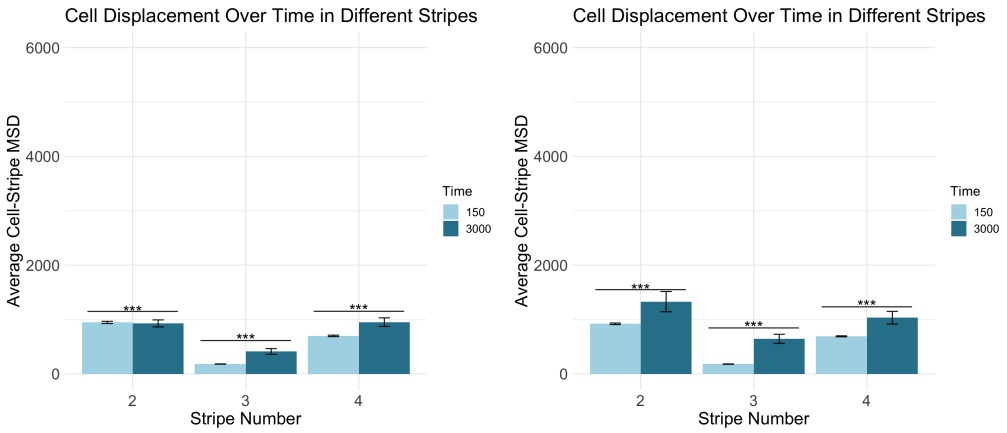

(a) $\lambda_{Act} = 1$, Periodic boundaries = TRUE (b) $\lambda_{Act} = 1$, Periodic boundaries = FALSE

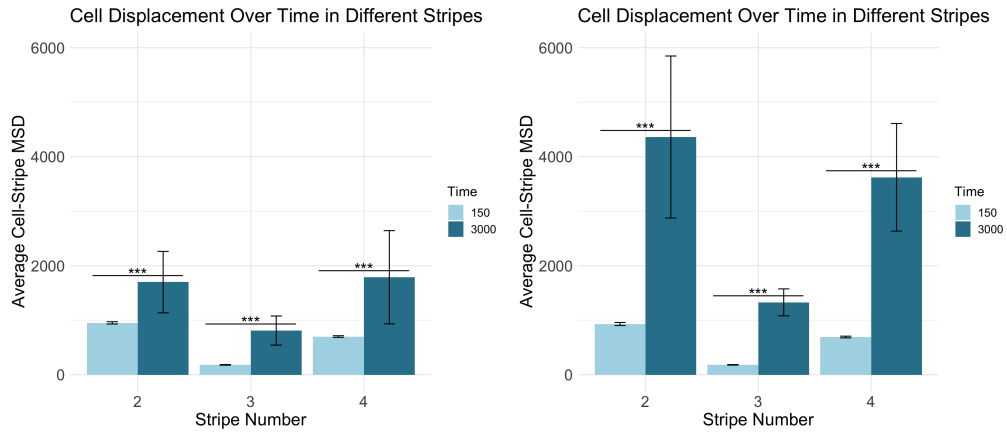

(c) $\lambda_{Act} = 160$, Periodic boundaries = TRUE (d) $\lambda_{Act} = 160$, Periodic boundaries = FALSE

Figure 5.11: **Under Run-and-Chase Dynamics, significant Cell Displacement occurs regardless of λ_{Act} and Boundary Conditions.** Four plots denoting the mean square displacement (MSD) of cells of stripe 2-4 from their original stripe axis at $t = 150$ and $t = 3000$. λ_{Act} was set to $\lambda_{Act} = 1$ (plot (a) and (b)) and $\lambda_{Act} = 160$ (plot (c) and (d)). Periodic boundaries were set to true (plot (a) and (c)) or false (plot (b) and (d)). For all sets of conditions, significant displacement occurs over time.

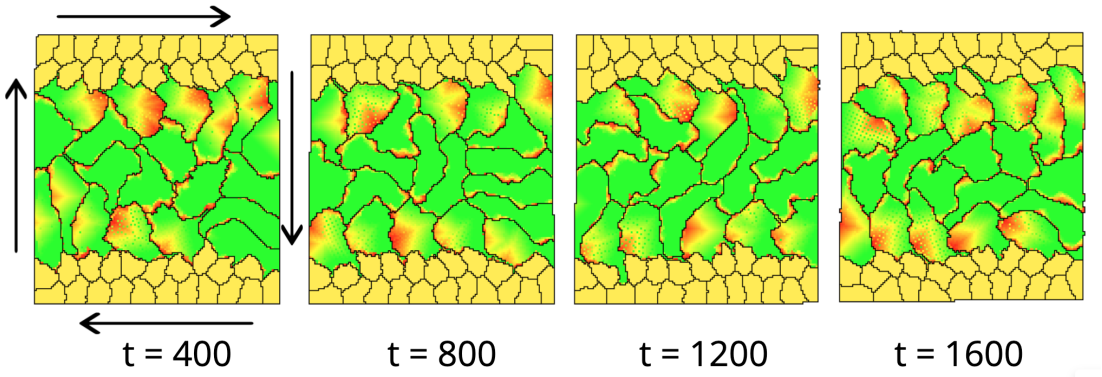

Figure 5.12: **Chiral Movement of Melanophore leads to the circulation of Melanophores within their Stripe.** A time-series of a striped pattern with xanthophores (yellow) and melanophores (green). The chiral repolarisation of the melanophores leads to them circling around within their stripe in a clockwise manner. Xanthophores maintain confied to their stripe.

These movement-patterns were not replicated when melanophore repolarisation was modeled to be not chiral, but to occur in random directions. Fig. 5.13 shows the resulting pattern when repolarisation was modelled to occur in random directions. The melanophores line up in thin stripes in order to minimize contact with xanthophores. Although this pattern is stable, it could be possible that *in vitro*, this would lead to melanophores crawling on top of each other and thus lead to tissue distortion. Thus, chiral melanophore movement leads to a unique cell cluster movement.

In Fig. 5.13, it is visible that the melanophores have an uneven distribution of Act values within them. This is due to the mechanism in which repolarisation is implemented; the algorithm that changes the Act values at times skips over adjacent sites. This is homogenized when repolarisation occurs in only one direction, since then the algorithm is called multiple times in adjacent location, which ensures that adjacent sites sites are filled. A method to circumvent this problem is addressed in the Discussion.

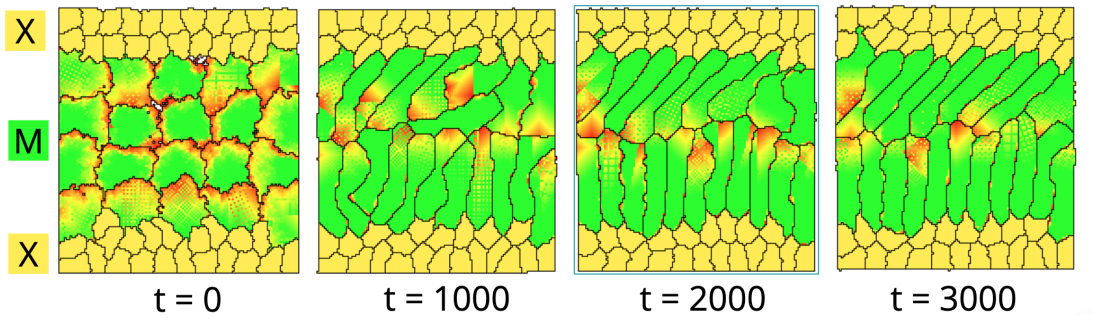

Figure 5.13: **When melanophores repolarise in random Directions, melanophore alignment occurs.** A time series of a simulation where run-and-chase dynamics were implemented whereby melanophore repolarisation was set to occur in random directions. By $t = 2000$, melanophores have aligned themselves to minimize contact with xanthophores.

Fig. 5.14 shows the result of 10 simulations run with $\lambda_{Act} = 1$. It is visible that the pattern is largely conserved, although sometimes the stripes do loose their straight shape or start mixing. This is confirmed by Fig. 5.15, which shows the MSD of cells from their original stripe axis. At $t = 3000$, this distance has significantly increased from $t = 150$, indicating that the original stripes are loosing their compact shape.

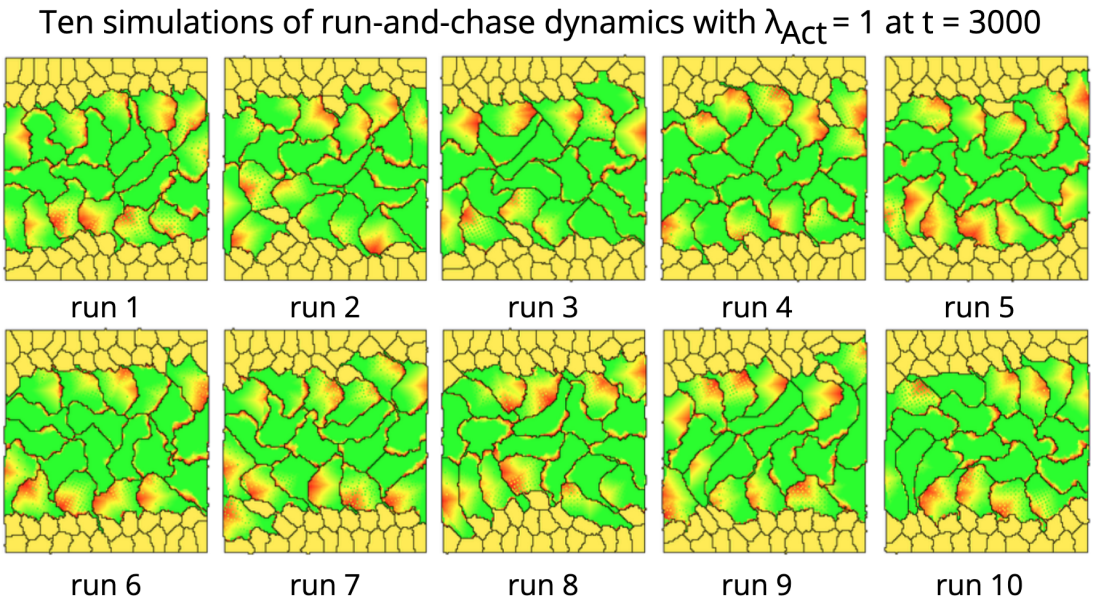

Figure 5.14: **Result of 10 simulations of run-and-chase dynamics with $\lambda_{Act} = 1$ at $t = 3000$.** .

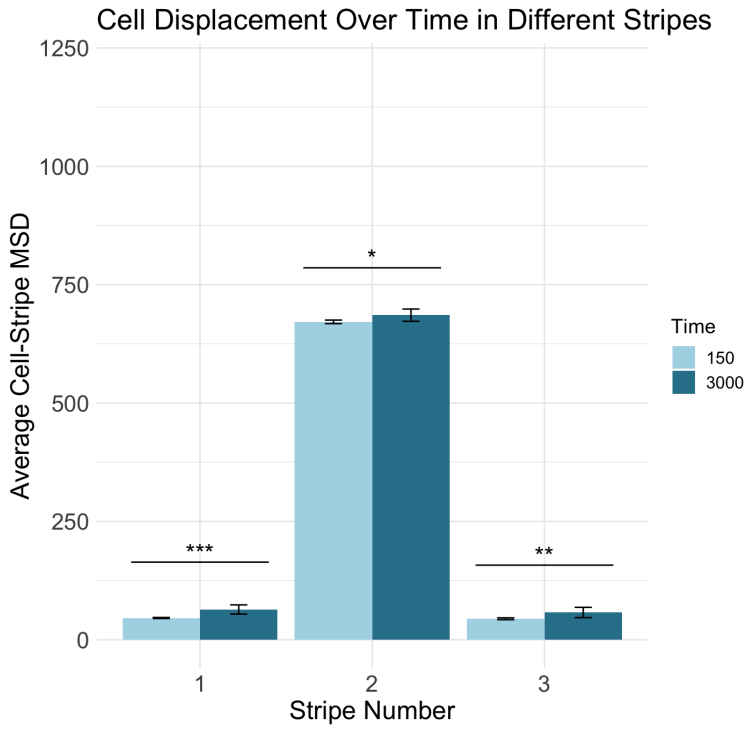

Figure 5.15: **Significant cell displacement occurs under run-and-chase dynamics.** Bar chart showing the mean square displacement (MSD) of cells from their original stripe axis. The difference between the MSD at $t = 150$ and $t = 3000$ significant for all three stripes, indicating that the pattern looses stability.

We contrasted our findings to what occurs when no interactions between xanthophores and melanophores are modelled. When $J_{M,X} = 12$, xanthophores quickly migrate into melanophore regions. When $J_{M,X} = 40$, the pattern was stable (Fig. 5.16). Fig. 5.17 shows the number

of xanthophores that are only in contact with melanophores at $t = 3000$. This number is significantly higher when $J_{MX} = 12$ than when $J_{MX} = 40$. Thus, low melanophore-xanthophore adhesion prevents stripe intermixing.

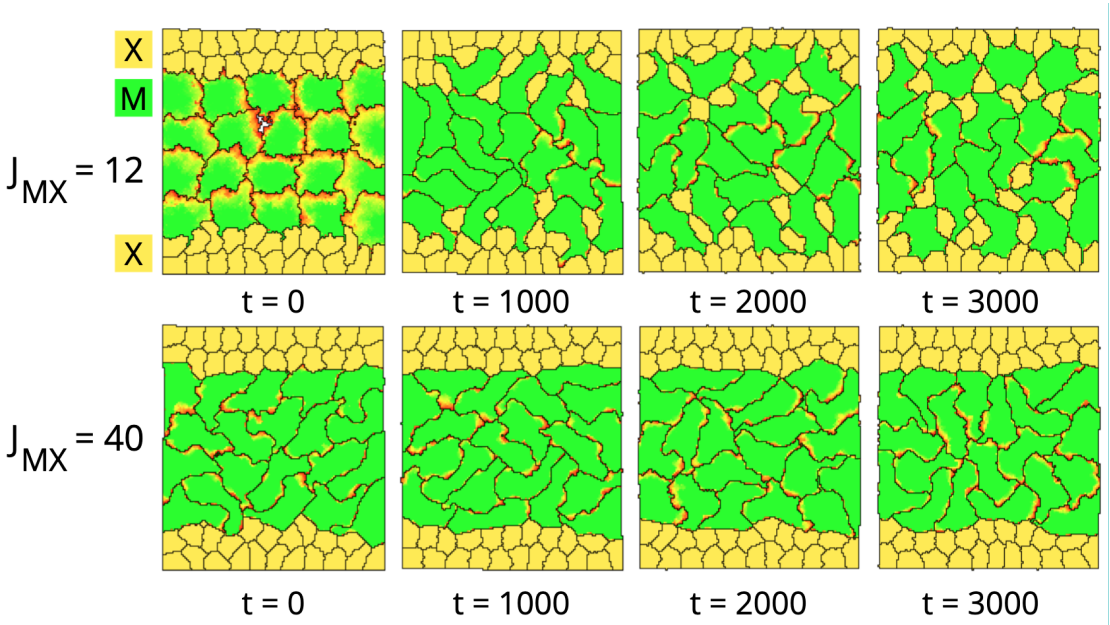

Figure 5.16: **High melanophore-xanthophore adhesion leads to cell intermixing.** Top) Time series of a melanophore-xanthophore interactions with $J_{MX} = 12$ and no run-and-chase dynamics implemented. At $t = 1000$, xanthophores are already breaking of from their stripe and move further into the melanophore stripe over time. Bottom) Time series of a melanophore-xanthophore interactions with $J_{MX} = 40$ and no run-and-chase dynamics implemented. Due to low melanophore-xanthophore adhesion, each celltype adheres to its own group.

Coming back to stripe formation, we simulated three melanophores and two xanthophore stripes in the same conditions as previously, but with $J_{MX} = 40$. Fig. 5.18 shows a time series of the resulting pattern. Unlike under run-and-chase dynamics, the pattern is completely stable and no cell intermixing occurs. This implies that chiral run-and-chase dynamics between melanophores and xanthophores may have a different function that pattern stabilization, since varying the cell-cell adhesion strength is a more reliable way to achieve stripe-pattern stability.

Ultimately, we conclude that chiral movement of melanophores leads to a unique clockwise movement of the melanophore cluster. This movement does not lead to stable patterns, since xanthophores still move into melanophore regions. Low melanophore-xanthophore adhesion already leads to stable stripe formation, which suggests that the chiral movement may have another biological function.

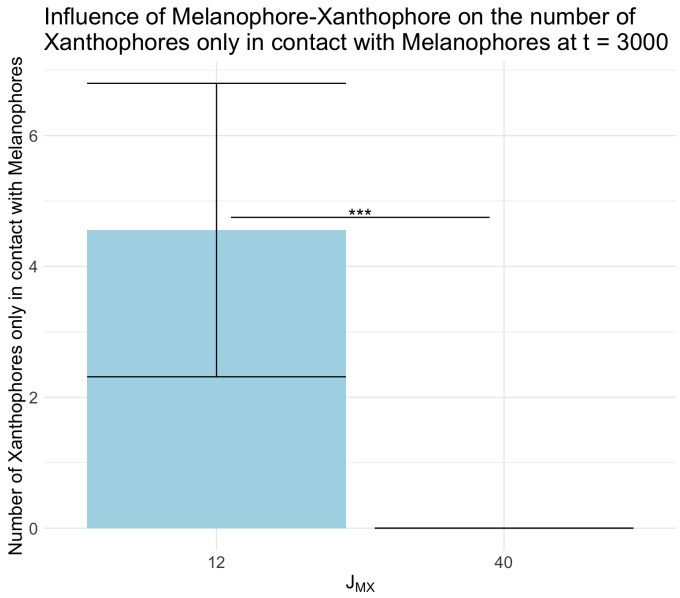

Figure 5.17: **High melanophore-xanthophore adhesion leads to xanthophore movement into melanophore regions.** The number of xanthophores only in contact with melanophores was recorded at $t = 3000$ for $J_{MX} = 12$ and $J_{MX} = 40$. For $J_{MX} = 40$, this number is 0, indicating that xanthophores adhere to their own stripe. For $J_{MX} = 12$ this number is significantly higher, indicating that xanthophore migration into melanophore regions occurs.

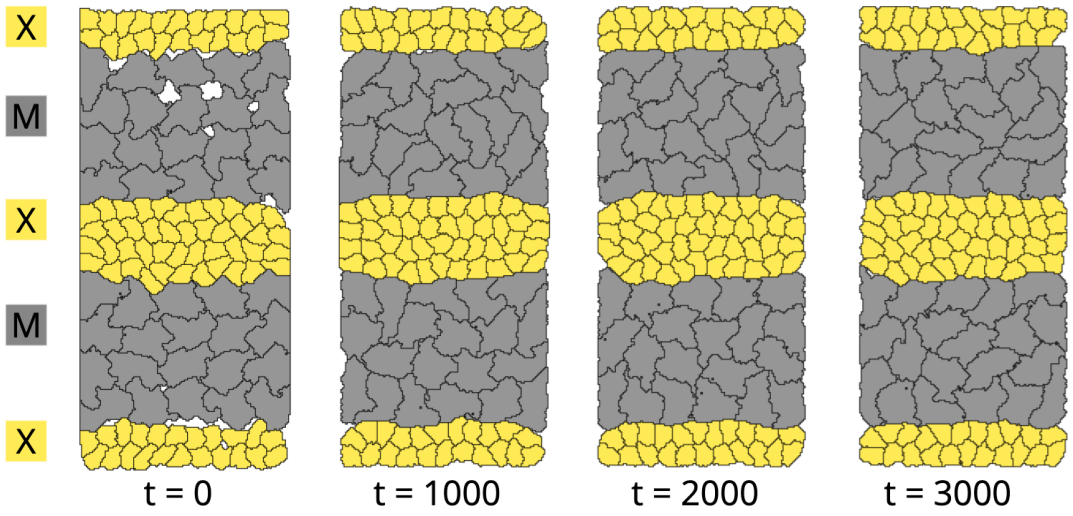

Figure 5.18: **High melanophore-xanthophore adhesion leads to stable stripe patterns.** A time series of stripe patterns of melanophores (grey) and xanthophores (yellow), from 0 to 3000 MCS. Simulations were performed with $J_{MX} = 40$.

Chapter 6

Discussion

In this work, we built a cellular Potts model of CIL. The model was able to mimic certain biological observations, such as the dispersal of circular cell clusters and run-and-chase dynamics between melanophores and xanthophores. The model was not able to replicate haemocyte dispersal patterns in *Drosophila*, presumably since lamellae extension by haemocytes significantly contributes to this dispersal. To model this behaviour, a cellular Potts extension which includes lamellae should be developed. This model would be useful for studying several pattern formation processes. For example, xanthophores extend long-range projections towards melanophores, which influence melanophore organization [24]. Incorporating long-range projections into our zebrafish stripes model could give a better understanding of when pattern stability could be achieved. Thus, there is room for subsequent work in this area.

It could be questioned whether our current model is truly simple. The repolarisation component of the model is computationally intensive, since it requires the iteration over many sites near the repolarisation site. A way to minimize this would be to perform experiments to find the minimal area near the repolarisation site that must be filled in order for repolarisation to occur. Additionally, perhaps it would be sufficient to only increase the Act value of sites that are located at the cell edge. These sites, after all, are those that contribute most to cell motility. This would also prevent the seemingly random distribution of Act values within the cells that occurs if repolarisation is set to occur in random directions (see Fig. 5.13). Overall, these two methods could be used to simplify the model.

Even without the repolarisation component, the current model is computationally intensive, since every timestep, we have to go through all lattice sites in order to find contact-sites between cells. A possible way to reduce the number of sites over which we have to iterate would be "memorize" where on the grid the last point of contact occurred. Then in subsequent timesteps, we could search for contact sites only these areas and not iterate over lattice sites which are away from cells. This method would require less iterations, but would still require memorization, which can also be computationally intensive. Thus, it is not yet clear what the optimal way is to perform the contact-site search. Solving this issue is important, since it would allow the model to run large simulations, such as simulations a larger number of zebrafish stripes.

An interesting finding that came up in the study is that the chiral movement of xanthophores does not have to be an incorporated into the model, but is an emergent property that occurs when melanophore movement is chiral. The role of these chiral movements was not elucidated in this work. Future work could resolve this question, by modeling chiral movement not only in stripe patterns, but in other patterns as well. This could show in which situations chiral movement may maintain pattern stability and therefore expose its role in biological systems.

In this work, only one type of zebrafish stripe pattern was considered (one containing four melanophores and four xanthophores per stripe). Therefore, we cannot completely rule out the possibility that run-and-chase dynamics occur *in vivo*, since they may occur when stripes have a different composition (for example, slightly broader or smaller stripes). Therefore, in subsequent work, a wider range of stripe composition should be tested. Additionally, no alternative hypothesis for the mode of interaction of melanophores and xanthophores was tested in this work. Therefore, there is the possibility that pattern stability was disrupted due to the experimental

setup and not due to the interactions we modelled. In further work, an alternative hypothesis should be added.

A future application of the model would be the study neural crest formation. In the first section of this study, we performed simulations that mimicked the behaviour of neural crest cells in a two-cell setting. This could be extended to a larger scale setting, in order to study patterns such as the migration of NC cell clusters towards placode cell clusters [25], the migration of NC cell clusters [26], and the formation of the neural crest as observed *in vivo* [2].

An extension to the model could be made by incorporating cell-matrix adhesions. This could be done by combining the current model with an Act CPM developed by Leonie et al. [27], which incorporates cell-matrix adhesions. Such a model could be used to answer questions such as; *What is the role of cell-matrix adhesions in CIL?* and *How does increased cell-matrix adhesion strength influence CIL?*

In conclusion, our model captures CIL dynamics and is able to reproduce a range of biological phenomena, such as cell cluster dispersal and run-and-chase dynamics. While the model shows promising results, there are areas for improvement in terms of computational complexity and model simplicity. There are also areas in which the model could be extended, for example by adding cell-matrix adhesions, which would allow new research questions to be answered. There is potential to use this model to further explore the mechanism of zebrafish stripe formation and the role of cell-chirality in biological patterns.

Appendix A

Parameters

Table A.1: Parameters and their values

Parameter	**Description**	**Value**
T	Temperature	20
A_{target}	Target area	500 px^2
λ_A	Weight area constraint	50
P_{target}	Target perimeter	340 px
λ_P	Weight perimeter constraint	2
λ_{Act}	Weight of Act model	120
MaxAct	Act lifetime	30
$J_{\text{medium,medium}}$	Adhesion energy between medium	0
$J_{\text{NC,medium}}$	Adhesion energy between cell and medium	16
$J_{\text{NC,NC}}$	Adhesion energy between cells	10
Total MCS	Simulation duration	3000 MCS

Table A.2: Parameters and their values for melanophore and xanthophore experiments

Parameter	**Description**	**Value for Xathophores**	**Value for Melanophores**
A_{target}	Target area	150 px^2	600 px^2
λ_A	Weight area constraint	50	50
P_{target}	Target perimeter	150 px	380 px
λ_P	Weight perimeter constraint	2	2
λ_{Act}	Weight of Act model	120	200
Max_{Act}	Act lifetime	30	30

Table A.3: Parameters and their values for melanophore and xanthophore experiments

Parameter	**Description**	**Value**
T	Temperature	20
$J_{medium,medium}$	Adhesion energy between medium	0
$J_{M,medium}$	Adhesion energy between melanophores and medium	16
$J_{M,M}$	Adhesion energy between melanophores	10
$J_{X,medium}$	Adhesion energy between xanthophores and medium	16
$J_{X,X}$	Adhesion energy between xanthophores	5
$J_{X,M}$	Adhesion energy between xanthophores and melanophores	16
Total MCS	Simulation duration	3000 MCS

Appendix B

Code

Bibliography

[1] B. Stramer and R. Mayor, "Mechanisms and in vivo functions of contact inhibition of locomotion," *Nature reviews Molecular cell biology*, vol. 18, no. 1, pp. 43–55, 2017.

[2] A. Szabó, E. Theveneau, M. Turan, and R. Mayor, "Neural crest streaming as an emergent property of tissue interactions during morphogenesis," *PLoS computational biology*, vol. 15, no. 4, p. e1007002, 2019.

[3] J. R. Davis, C.-Y. Huang, J. Zanet, S. Harrison, E. Rosten, S. Cox, D. Y. Soong, G. A. Dunn, and B. M. Stramer, "Emergence of embryonic pattern through contact inhibition of locomotion," *Development*, vol. 139, no. 24, pp. 4555–4560, 2012.

[4] D. M. Parichy, "Pigment patterns: fish in stripes and spots," *Current Biology*, vol. 13, no. 24, pp. R947–R950, 2003.

[5] D. A. Kulawiak, B. A. Camley, and W.-J. Rappel, "Modeling contact inhibition of locomotion of colliding cells migrating on micropatterned substrates," *PLoS computational biology*, vol. 12, no. 12, p. e1005239, 2016.

[6] N. Rojas, A. Zuñiga, and P. Encina, "Pattern formation via cell–cell adhesion and contact inhibition of locomotion in active matter," *AIP Advances*, vol. 13, no. 2, 2023.

[7] A. Szabó, M. Melchionda, G. Nastasi, M. L. Woods, S. Campo, R. Perris, and R. Mayor, "In vivo confinement promotes collective migration of neural crest cells," *Journal of Cell Biology*, vol. 213, no. 5, pp. 543–555, 2016.

[8] I. Niculescu, J. Textor, and R. J. De Boer, "Crawling and gliding: a computational model for shape-driven cell migration," *PLoS computational biology*, vol. 11, no. 10, p. e1004280, 2015.

[9] H. Yamanaka and S. Kondo, "In vitro analysis suggests that difference in cell movement during direct interaction can generate various pigment patterns in vivo," *Proceedings of the National Academy of Sciences*, vol. 111, no. 5, pp. 1867–1872, 2014.

[10] J. P. Owen, R. N. Kelsh, and C. A. Yates, "A quantitative modelling approach to zebrafish pigment pattern formation," *Elife*, vol. 9, p. e52998, 2020.

[11] A. Volkening and B. Sandstede, "Modelling stripe formation in zebrafish: an agent-based approach," *Journal of the Royal Society Interface*, vol. 12, no. 112, p. 20150812, 2015.

[12] T. E. Woolley, P. K. Maini, and E. A. Gaffney, "Is pigment cell pattern formation in zebrafish a game of cops and robbers?," *Pigment Cell & Melanoma Research*, vol. 27, no. 5, pp. 686–687, 2014.

[13] H. Yamanaka and S. Kondo, "Zebrafish melanophores suggest novel functions of cell chirality in tissue formation," *Symmetry*, vol. 13, no. 1, p. 130, 2021.

[14] R. Mayor and C. Carmona-Fontaine, "Keeping in touch with contact inhibition of locomotion," *Trends in cell biology*, vol. 20, no. 6, pp. 319–328, 2010.

[15] M. Inaba, H. Yamanaka, and S. Kondo, "Pigment pattern formation by contact-dependent depolarization," *Science*, vol. 335, no. 6069, pp. 677–677, 2012.

[16] F. Graner and J. A. Glazier, "Simulation of biological cell sorting using a two-dimensional extended potts model," *Physical review letters*, vol. 69, no. 13, p. 2013, 1992.

[17] R. A. Desai, S. B. Gopal, S. Chen, and C. S. Chen, "Contact inhibition of locomotion probabilities drive solitary versus collective cell migration," *Journal of The Royal Society Interface*, vol. 10, no. 88, p. 20130717, 2013.

[18] M. R. Clay and M. C. Halloran, "Control of neural crest cell behavior and migration: insights from live imaging," *Cell adhesion & migration*, vol. 4, no. 4, pp. 586–594, 2010.

[19] E. Scarpa, A. Roycroft, E. Theveneau, E. Terriac, M. Piel, and R. Mayor, "A novel method to study contact inhibition of locomotion using micropatterned substrates," *Biology open*, vol. 2, no. 9, pp. 901–906, 2013.

[20] P. J. Van Haastert, "Amoeboid cells use protrusions for walking, gliding and swimming," *PloS one*, vol. 6, no. 11, p. e27532, 2011.

[21] J. Moreira and A. Deutsch, "Pigment pattern formation in zebrafish during late larval stages: A model based on local interactions," *Developmental dynamics: an official publication of the American Association of Anatomists*, vol. 232, no. 1, pp. 33–42, 2005.

[22] E. Scarpa, A. Szabó, A. Bibonne, E. Theveneau, M. Parsons, and R. Mayor, "Cadherin switch during emt in neural crest cells leads to contact inhibition of locomotion via repolarization of forces," *Developmental cell*, vol. 34, no. 4, pp. 421–434, 2015.

[23] G. Takahashi and S. Kondo, "Melanophores in the stripes of adult zebrafish do not have the nature to gather, but disperse when they have the space to move," *Pigment cell & melanoma research*, vol. 21, no. 6, pp. 677–686, 2008.

[24] D. S. Eom, E. J. Bain, L. B. Patterson, M. E. Grout, and D. M. Parichy, "Long-distance communication by specialized cellular projections during pigment pattern development and evolution," *Elife*, vol. 4, p. e12401, 2015.

[25] E. Theveneau, B. Steventon, E. Scarpa, S. Garcia, X. Trepat, A. Streit, and R. Mayor, "Chase-and-run between adjacent cell populations promotes directional collective migration," *Nature cell biology*, vol. 15, no. 7, pp. 763–772, 2013.

[26] A. Szabó and R. Mayor, "Modelling collective cell migration of neural crest," *Current opinion in cell biology*, vol. 42, pp. 22–28, 2016.

[27] L. van Steijn, I. M. Wortel, C. Sire, L. Dupré, G. Theraulaz, and R. M. Merks, "Computational modelling of cell motility modes emerging from cell-matrix adhesion dynamics," *PLoS computational biology*, vol. 18, no. 2, p. e1009156, 2022.